

Structure Learning in Inverse Ising Problems Using ℓ_2 -Regularized Linear Estimator

Xiangming Meng

*Institute for Physics of Intelligence and Department of Physics
Graduate School of Science
The University of Tokyo
7-3-1, Hongo, Tokyo 113-0033, Japan*

MENG@G.ECC.U-TOKYO.AC.JP

Tomoyuki Obuchi

*Department of Systems Science
Graduate School of Informatics
Kyoto University
Yoshida Hon-machi, Sakyo-ku, Kyoto-shi, Kyoto 606-8501, Japan*

OBUCHI@I.KYOTO-U.AC.JP

Yoshiyuki Kabashima

*Institute for Physics of Intelligence and Department of Physics
Graduate School of Science
The University of Tokyo
7-3-1, Hongo, Tokyo 113-0033, Japan*

KABA@PHYS.S.U-TOKYO.AC.JP

Abstract

Inferring interaction parameters from observed data is a ubiquitous requirement in various fields of science and engineering. Recent studies have shown that the pseudolikelihood (PL) method is highly effective in meeting this requirement even though the maximum likelihood method is computationally intractable when used directly. To the best of our knowledge, most existing studies assume that the postulated model used in the inference stage covers the true model that generates the data. However, such an assumption does not necessarily hold in practical situations. From this perspective, we discuss the utility of the PL method in model mismatch cases. Specifically, we examine the inference performance of the PL method when ℓ_2 -regularized (ridge) linear regression is applied to data generated from sparse Boltzmann machines of Ising spins using methods of statistical mechanics. Our analysis indicates that despite the model mismatch, one can perfectly identify the network topology using naive linear regression without regularization when the dataset size M is greater than the number of Ising spins, N . Further, even when $M < N$, perfect identification is possible using a two-stage estimator with much better quantitative performance compared to naive usage of the PL method. Results of extensive numerical experiments support our findings.

Keywords: inverse Ising problems, structure learning, model mismatch, pseudolikelihood method, replica method

1. Introduction

The advent of massive data across various scientific disciplines has led to widespread use of the classical Ising model as a tool for data modeling (Nguyen et al., 2017). Recent applications that have spurred this trend include retinal neurons, reconstruction of neural and gene regulatory networks, and determination of the three-dimensional structure of proteins in biological sciences (Aurell and Ekeberg, 2012; Bachschmid-Romano and Opper, 2015; Nguyen et al., 2017; Berg, 2017; Bachschmid-Romano and Opper, 2017; Abbara et al., 2020). Inference based on the Ising model is called the inverse Ising problem or Boltzmann machine learning, which refers to reconstructing the parameters and structure of an Ising model on the basis of samples of spin configurations. The maximum likelihood (ML) method is one of the main methods for solving this problem. However, in general, ML is computationally intractable for a large system. Two popular approaches have been developed to address this problem. The first is to approximate the ML using approximations such as Monte Carlo sampling (Ackley et al., 1985; Habeck, 2014; Broderick et al., 2007) and mean-field approximations (Kappen and Rodríguez, 1998; Tanaka, 1998; Sessak and Monasson, 2009). The second approach introduces some local cost function that is easier to optimize instead of directly maximizing the likelihood function. One of the most effective examples of the latter is the pseudolikelihood (PL) method (Besag, 1975; Aurell and Ekeberg, 2012; Decelle and Ricci-Tersenghi, 2014; Mozeika et al., 2014), which approximates the likelihood function as the product of conditional likelihood functions. A prominent advantage of the PL method is that one can independently estimate the couplings associated with each spin, as the local couplings directly connected to a single spin are isolated from the others, thus simplifying the implementation.

Recently, some theoretical analyses using methods of statistical mechanics have revealed the tight limit of inference accuracy in the large system limit, where the number of spins approaches infinity and the dataset size is comparable to the model dimensionality. Such analyses of the typical performance provide a firm theoretical basis for inverse Ising problems (Bachschmid-Romano and Opper, 2015, 2017; Berg, 2017; Abbara et al., 2020). For example, in Bachschmid-Romano and Opper (2017), assuming that data are drawn independently from an equilibrium Ising model, the learning performance of the PL method with a local cost function was studied for fully connected Ising models using a combination of the replica method and the cavity method (Mezard and Montanari, 2009; Opper and Saad, 2001; Nishimori, 2001). Subsequently, in Abbara et al. (2020), the authors extended the analysis to sparse coupling, i.e., sparse Boltzmann machines, which is expected to provide clearer interpretations and has wide practical applications in structure learning of graphical models (Schmidt et al., 2007; Wainwright and Jordan, 2008; Ravikumar et al., 2010; Santhanam and Wainwright, 2012; Aurell and Ekeberg, 2012; Decelle and Ricci-Tersenghi, 2014; Bresler, 2015; Vuffray et al., 2016; Lokhov et al., 2018). Notably, rigorous analysis of information-theoretical results has been presented in Santhanam and Wainwright (2012). To the best of our knowledge, most existing studies assume that the postulated model used

in the inference stage covers the true model that generates the data. However, such an assumption does not necessarily hold in practical situations, because the model generating the data is generally unknown *a priori*. Therefore, it is important to evaluate the learning performance of the popular PL method in model mismatch cases, which is the main focus of this study.

Specifically, within the teacher-student framework, we examine the inference (learning) performance of the PL method when ℓ_2 -regularized (ridge) linear regression is applied to data generated from sparse Boltzmann machines of Ising spins using methods of statistical mechanics. We focus on the ℓ_2 regularizer because, in addition to being a typical example of model mismatch cases, it is computationally efficient. Although the required computational costs of the ℓ_1 and ℓ_2 approaches are of the same order in the sense of theoretical computer science, the cost of the ℓ_2 regularizer is much lower than that of the ℓ_1 regularizer in practice, as its estimator can be expressed in a closed form. Therefore, clarifying its possibilities and limitations is important for practical purposes. It is shown that in the large system limit, i.e., where the number of Ising spins N approaches infinity while the number of observations, M , is proportional to N , the learning performance can be characterized by several macroscopic variables, from which several interesting observations are made. First, without regularization, the linear regression estimator is unbiased in the inactive set of teacher couplings so that perfect recovery of the structure is possible even under model mismatch. However, as with Bachschmid-Romano and Opper (2017); Abbara et al. (2020), the residual sum of squares (RSS) diverges significantly when the measurement ratio $\alpha = M/N \rightarrow 1$, which makes the result uninformative in the region $\alpha \leq 1$. Second, although ℓ_2 -regularized (ridge) linear regression successfully overcomes the problem of divergence, it introduces additional nonzero mean estimates in the inactive set of teacher couplings. Consequently, when using ℓ_2 regularization, one must carefully choose a certain threshold to avoid possible false positives, which is difficult though not impossible in the large system limit. It is proved that for any spin s_0 selected in the PL method, the nonzero biases in the inactive set of teacher couplings decay exponentially fast with respect to (w.r.t.) the distance from s_0 . Inspired by this observation, we propose the following two-stage estimation approach for structure learning. In the first stage, ridge regression is adopted to select a set of $\mathcal{O}(1)$ potential active couplings via comparison with a certain threshold¹. In the second stage, linear regression (without regularization) is adopted to further eliminate the possible false positives. As the second stage corresponds to a situation with an infinite measurement ratio in the large system limit, perfect reconstruction will be guaranteed. This result supports the underlying possibility of perfect structure learning for inverse Ising problems in the presence of model mismatch, even when the data size is smaller than the number of Ising spins. Numerical experiments conducted on locally tree-like graphs, such as the random regular (RR) graph and the Erdős–Rényi (ER) graph, verify the validity

1. To facilitate perfect recovery of the structure, this threshold should be sufficiently small to ensure full recall.

of the theoretical analysis and two-stage estimator in structure learning in inverse Ising problems.

The remainder of this paper is organized as follows. Section 2 reviews inverse Ising problems and the PL method. In addition, it presents the mismatched ℓ_2 -regularized linear estimator to be analyzed. Section 3 describes the statistical mechanics analysis of the ℓ_2 -regularized linear estimator, drawing on previous studies (Bachschmid-Romano and Oppen, 2017; Abbara et al., 2020) for sparse couplings. Numerical simulations are conducted to evaluate the accuracy of the theoretical analysis, and Section 5 compares the experimental results with the theoretical analysis. Finally, Section 6 concludes the paper.

2. Inverse Ising Problem

Consider an Ising model with N binary spin variables $\mathbf{s} = (s_i = \pm 1)_{i=0}^{N-1}$, which follows the Boltzmann distribution

$$P_{\text{Ising}}(\mathbf{s}|\mathbf{J}, \mathbf{H}) = \frac{1}{Z_{\text{Ising}}} e^{\sum_{i<j} J_{ij} s_i s_j + \sum_i H_i s_i}, \quad (1)$$

where Z_{Ising} is the partition function and $\mathbf{J} = (J_{ij})_{ij} \in \mathbb{R}^{N \times N}$ and $\mathbf{H} = (H_i)_{i=0}^{N-1} \in \mathbb{R}^N$ are the couplings and external fields, respectively. In (1), the temperature is absorbed in \mathbf{J} and \mathbf{H} . In practical applications, the underlying structure and the values of the couplings are usually unknown a priori, and they must be inferred through observations. The goal of the inverse Ising problem is to learn the couplings \mathbf{J} and external fields \mathbf{H} from a set of observations of spin snapshots $\mathcal{D}^M = \{\mathbf{s}^{(\mu)}\}_{\mu=1}^M$, where M denotes the number of samples in the dataset. A standard approach to address this problem is the maximum likelihood (ML) method, defined as

$$\left\{ \hat{\mathbf{J}}^{ML}, \hat{\mathbf{H}}^{ML} \right\} = \arg \min_{\mathbf{J}, \mathbf{H}} \left\{ - \sum_{\mu=1}^M \log P_{\text{Ising}}(\mathbf{s}^{(\mu)}|\mathbf{J}, \mathbf{H}) \right\}. \quad (2)$$

Despite its useful properties of consistency and asymptotic efficiency, the ML method suffers from exponentially high computational complexity, i.e., it becomes intractable, for large N . Monte Carlo (MC)-based approximation can be used as in Ackley et al. (1985) to alleviate this problem, but it requires a long time to reach equilibration, although it is asymptotically exact as the number of MC steps approaches infinity.

2.1 Pseudolikelihood Method

Instead of directly minimizing the global negative log likelihood as in (2), an alternative approach is the pseudolikelihood (PL) method (Besag, 1975), which replaces the original likelihood with the conditional distribution $P(s_i|\mathbf{s}_{\setminus i}, \mathbf{J}_i, H_i)$ for each spin s_i , where $\mathbf{J}_i =$

$(J_{ij})_{j=0, j \neq i}^{N-1}$ is the coupling vector connected to spin s_i and $\mathbf{s}_{\setminus i}$ is the spin vector \mathbf{s} excluding s_i . Specifically, for each i , the conditional distribution $P(s_i | \mathbf{s}_{\setminus i}, \mathbf{J}_i, H_i)$ is of the form

$$P(s_i | \mathbf{s}_{\setminus i}, \mathbf{J}_i, H_i) = \frac{1}{Z_i} e^{s_i (\sum_{j \neq i} J_{ij} s_j + H_i)}, \quad (3)$$

where $Z_i = 2 \cosh(\sum_{j \neq i} J_{ij} s_j + H_i)$ is the site partition function. Consequently, the PL estimator is applied to each i separately, leading to

$$\begin{aligned} \{\hat{\mathbf{J}}_i^{PL}, \hat{H}_i^{PL}\} &= \arg \min_{\mathbf{J}_i, H_i} \left\{ - \sum_{\mu=1}^M \log P(s_i^{(\mu)} | \mathbf{s}_{\setminus i}^{(\mu)}, \mathbf{J}_i, H_i) \right\} \\ &= \arg \min_{\mathbf{J}_i, H_i} \left\{ \sum_{\mu=1}^M l^{PL}(s_i^{(\mu)} | \mathbf{s}_{\setminus i}^{(\mu)}, \mathbf{J}_i, H_i) \right\}, \end{aligned} \quad (4)$$

where

$$l^{PL}(s_i^{(\mu)} | \mathbf{s}_{\setminus i}^{(\mu)}, \mathbf{J}_i, H_i) = \sum_{j \neq i} J_{ij} s_j + H_i, \quad (5)$$

and $l^{PL}(x) = -x + \log 2 \cosh x$ denotes the local cost function used in the PL method.

The PL method has two remarkable properties: consistency and locality (Hyvärinen, 2006). Consistency means that the PL estimator converges to the true value when the dataset size M is sufficiently large. Locality means that each coupling vector \mathbf{J}_i can be estimated independently, which leads to low computational complexity but results in the loss of coupling symmetry ($\hat{J}_{ij}^{PL} \neq \hat{J}_{ji}^{PL}$ in general). Consequently, the PL method transforms the original complicated inverse Ising inference problem into parallel independent nonlinear (generalized linear) inference problems (4).

2.2 Mismatched Teacher-Student Scenario with Sparse Couplings

Consider the inverse Ising problem in the teacher-student scenario, where the dataset $\mathcal{D}^M = \{\mathbf{s}^{(\mu)}\}_{\mu=1}^M$ is assumed to be generated independently from a teacher Ising model with couplings \mathbf{J}^* and external fields \mathbf{H}^* . For simplicity, the external fields are assumed to be zero, i.e., $\mathbf{H}^* = 0$. The aim of the student network is to infer the teacher couplings \mathbf{J}^* from the dataset \mathcal{D}^M . Then, a critical question is how many observations are required or what is the dataset size \mathcal{D}^M required for the student network to achieve a certain level of reconstruction performance. Such a problem can be addressed by investigating the learning curve, i.e., the average reconstruction error of the student network as a function of the measurement ratio $\alpha = M/N$. Specifically, the average reconstruction error is characterized by

the average residual sum of square (RSS)

$$\mathcal{E} = \left[\left\| \mathbf{J}_i^* - \hat{\mathbf{J}}_i \right\|_2^2 \right]_{\mathcal{D}^M}, \quad (6)$$

where $[\cdot]_{\mathcal{D}^M}$ denotes the expectation over the ensemble of M training data \mathcal{D}^M drawn randomly from an Ising model with teacher couplings \mathbf{J}^* , i.e.,

$$[\cdot]_{\mathcal{D}^M} = \sum_{\mathbf{s}^{(1)}, \dots, \mathbf{s}^{(M)}} (\cdot) \prod_{\mu=1}^M P_{\text{Ising}}(\mathbf{s}^{(\mu)} | \mathbf{J}^*). \quad (7)$$

Before delving into their calculation, two important issues are considered. First, one has to specify the student network to infer the teacher couplings. Ideally, the student model is expected to exactly match the true teacher model generating the data, which is not necessarily the case in most real-world applications. Therefore, it is intriguing to analyze the learning performance with model mismatch. Second, in high-dimensional settings, it is plausible to assume that the couplings of the teacher model are sparse, i.e., the corresponding topology of the teacher network is a sparsely connected graph rather than a fully connected one; otherwise, extracting useful information from data of practically accessible sizes is impossible. Consequently, the main focus of this study is to analyze the learning curve of the mismatched student model for teacher networks with sparse couplings.

Specifically, consider a simple ℓ_2 -regularized linear regression estimator, which is also widely known as ridge regression. In such cases, instead of the true local cost function $l^{PL}(x)$ of the teacher model defined in (5), a regularized quadratic cost function is used by the student network, i.e.,

$$l\left(s_i^{(\mu)} h_i\left(\mathbf{s}_{\setminus i}^{(\mu)}, \mathbf{J}_i\right)\right) = \left(s_i^{(\mu)} - \sum_{j \neq i} J_{ij} s_j^{(\mu)}\right)^2 + \frac{\lambda}{\alpha} \sum_{j \neq i} J_{ij}^2, \quad (8)$$

where $\lambda \geq 0$ is the ℓ_2 regularization coefficient. Using the regularized local loss (8), the corresponding optimization problem in (4) is now formulated as

$$\begin{aligned} \hat{\mathbf{J}}_i &= \arg \min_{\mathbf{J}_i} \left\{ \sum_{\mu=1}^M l\left(s_i^{(\mu)} h_i\left(\mathbf{s}_{\setminus i}^{(\mu)}, \mathbf{J}_i\right)\right) \right\} \\ &= \arg \min_{\mathbf{J}_i} \left\{ \sum_{\mu=1}^M \left(s_i^{(\mu)} - \sum_{j \neq i} J_{ij} s_j^{(\mu)}\right)^2 + \lambda N \sum_{j \neq i} J_{ij}^2 \right\} \\ &= \arg \min_{\mathbf{J}_i} \left\{ \|\mathbf{s}_i - \mathbf{A} \mathbf{J}_i\|_2^2 + \lambda N \|\mathbf{J}_i\|_2^2 \right\}, \end{aligned} \quad (9)$$

where $\mathbf{s}_i = \left(s_i^{(\mu)} \right)_{\mu=1}^M \in \mathbb{R}^{M \times 1}$, and $\mathbf{A} = \left(s_j^{(\mu)} \right)_{\mu, j \neq i} \in \mathbb{R}^{M \times (N-1)}$. Note that in (9), a factor N is introduced owing to the scaling of \mathbf{J}_i . Then, standard optimization methods for the ridge regression can be used by the student network.

3. Statistical Mechanics Analysis

In this section, we present the statistical mechanics analysis of the inference (learning) performance of the mismatched ℓ_2 -regularized linear estimator in (9) by drawing on previous studies (Bachschmid-Romano and Oppen, 2017; Abbara et al., 2020). For simplicity and without loss of generality, we focus on inferring the coupling vector \mathbf{J}_0 for spin s_0 . Hereafter, the subscript for \mathbf{J}_0 is omitted for notational simplicity. The basic idea of statistical mechanics analysis is to construct a Gibbs distribution of the student couplings using a Hamiltonian associated with the cost function of the student network. Specifically, from (9), we introduce the Hamiltonian

$$\begin{aligned} \mathcal{H}(\mathbf{J}|\mathcal{D}^M) &= \sum_{\mu=1}^M \left(s_0^{(\mu)} - \sum_{j=1}^{N-1} J_j s_j^{(\mu)} \right)^2 + \lambda N \sum_{j=1}^{N-1} J_j^2 \\ &= \sum_{\mu=1}^M \Phi \left(s_0^{(\mu)} h^{(\mu)} \right) + \lambda N \sum_{j=1}^{N-1} J_j^2, \end{aligned} \quad (10)$$

where $\Phi(x) = (x-1)^2$ and $h^{(\mu)} = \sum_{j=1}^{N-1} J_j s_j^{(\mu)}$. Then, the Gibbs distribution of the student couplings is defined as

$$P(\mathbf{J}|\mathcal{D}^M) = \frac{1}{Z} \exp[-\beta \mathcal{H}(\mathbf{J}|\mathcal{D}^M)], \quad (11)$$

where β represents the inverse temperature and Z is the partition function

$$Z = \int d\mathbf{W} \exp[-\beta \mathcal{H}(\mathbf{J}|\mathcal{D}^M)]. \quad (12)$$

Using techniques from statistical physics of disordered systems, one can first compute the partition function at nonzero temperature and then perform the limit $\beta \rightarrow +\infty$ at the end of the calculation. The thermal average $\langle \mathbf{J} \rangle$ w.r.t. the Gibbs distribution (11) converges to the minimizer of the cost function $\mathcal{H}(\mathbf{J}|\mathcal{D}^M)$, which is the solution to the local learning problem in (9). Macroscopic parameters can be extracted from the quenched average of the free energy density f corresponding to the expectation over the ensembles of the training dataset \mathcal{D}^M drawn randomly from an Ising model with teacher couplings \mathbf{J}^* , i.e.,

$$f = -\frac{1}{N\beta} [\log Z]_{\mathcal{D}^M}. \quad (13)$$

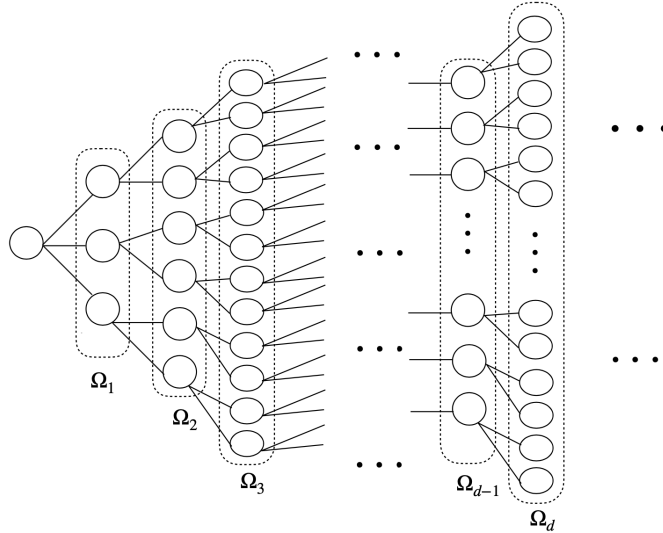


Figure 1: Schematic of nearest neighbor (NN) spins. In general, the d -th generation of spin s_0 is denoted as Ω_d , whose distance from spin s_0 is d .

Using the replica method, the free energy density can be computed as the limit form

$$f = -\frac{1}{N\beta} [\log Z]_{\mathcal{D}^M} = -\lim_{n \rightarrow 0} \frac{1}{N\beta} \frac{\partial}{\partial n} \log [Z^n]_{\mathcal{D}^M}, \quad (14)$$

$$[Z^n]_{\mathcal{D}^M} = \int \prod_{a=1}^n d\mathbf{J}^a e^{-\lambda N \sum_{a=1}^n \|\mathbf{J}^a\|_2^2} \left\{ \sum_{\mathbf{s}} P_{\text{Ising}}(\mathbf{s} | \mathbf{J}^*) \exp \left[-\beta \sum_{a=1}^n \Phi(s_0 h^a) \right] \right\}^{\alpha N}, \quad (15)$$

where $P_{\text{Ising}}(\mathbf{s} | \mathbf{J}^*)$ is the Boltzmann distribution of the teacher network in (1) with external fields $\mathbf{H}^* = 0$. Thus, the remaining task is to calculate $[Z^n]_{\mathcal{D}^M}$ in (15).

3.1 Sparse Ansatz with ℓ_2 Regularization

To calculate the integration in (15), we resort to the cavity approach originally proposed in Bachschmid-Romano and Opper (2017). However, as discussed in Abbara et al. (2020), the cavity field $h^a = \sum_j J_j^a s_j$ can no longer be regarded as a Gaussian in the sparse coupling case. To address this problem, we propose an ansatz similar to Abbara et al. (2020), by which the cavity field is decomposed into a signal part and a noise part. The noise part can then be modeled as a Gaussian using the central limit theorem, which enables us to obtain a solution.

Specifically, as an example case, we focus on a tree-like regular graph with degree c , and consider a sparse coupling teacher system where the zeroth spin s_0 is directly connected

to $c = \mathcal{O}(1)$ nearest-neighbor (NN) spins, whose index set is denoted as $\Omega_1 = \{i | J_i^* \neq 0, i \in \{1, \dots, N-1\}\}$. The spins in Ω_1 can be regarded as the first generation spins of spin s_0 in the sparse teacher system. Moreover, each spin in Ω_1 will be further connected to $c-1 = \mathcal{O}(1)$ NN spins except s_0 , all of which, denoted as Ω_2 , can be regarded as the second generation spins of s_0 . In general, the d -th generation of spin s_0 is denoted as Ω_d , which is graphically represented in Fig. 1. Denoting $\Psi_d = \{\Omega_1, \Omega_2, \dots, \Omega_d\}$ as the set of truncated NN spins up to generation $d = \mathcal{O}(1)$, and $\bar{\Psi}_d$ as the complementary set of Ψ_d , i.e., $\bar{\Psi}_d = \{i | i \notin \Psi_d, i \in \{1, \dots, N-1\}\}$, we assume that the estimates $\hat{\mathbf{J}} = \left(\hat{J}_i\right)_{i=1}^{N-1}$ obtained from the ℓ_2 -regularized estimator obey the following form:

$$\hat{J}_i = \begin{cases} \bar{J}_i + \frac{1}{\sqrt{N}} \Delta_i, & i \in \Psi_d, \\ \frac{1}{\sqrt{N}} \Delta_i, & i \in \bar{\Psi}_d, \end{cases} \quad (16)$$

where Δ_i is a random variable that has asymptotically zero mean with variance scaled as $\mathcal{O}(1)$. Note that the ansatz in (16) is a generalization of the ansatz in Abbbara et al. (2020), which only considers $\Psi_d = \Omega_1$ as the special case. The application range of this ansatz is discussed in Section 3.4. According to the ansatz in (16), the cavity field $h^a = \sum_j J_j^a s_j$ can be rewritten as the sum of the ‘‘signal’’ part h_{Ψ_d} and the ‘‘noise’’ part h_{Δ}^a :

$$h^a = h_{\Psi_d} + h_{\Delta}^a, \quad (17)$$

$$h_{\Psi_d} \doteq \sum_{j \in \Psi_d} \bar{J}_j s_j, \quad (18)$$

$$h_{\Delta}^a \doteq \frac{1}{\sqrt{N}} \sum_j \Delta_j^a s_j \approx \frac{1}{\sqrt{N}} \sum_{j \in \bar{\Psi}_d} \Delta_j^a s_j, \quad (19)$$

where the approximation in (19) is due to the assumption that there are only finite $\mathcal{O}(1)$ terms in Ψ_d , which are negligible in the large system limit, as discussed in Section 3.4. Moreover, the ℓ_2 norm square of $\mathbf{J}^a = \left(J_j^a\right)_j$ can be computed as

$$\begin{aligned} \|\mathbf{J}^a\|^2 &= \sum_{j \in \Psi_d} \left(\bar{J}_j^2 + 2\bar{J}_j \frac{\Delta_j^a}{\sqrt{N}} + \frac{(\Delta_j^a)^2}{N} \right) + \frac{1}{N} \sum_{j \in \bar{\Psi}_d} (\Delta_j^a)^2 \\ &\approx \sum_{j \in \Psi_d} \bar{J}_j^2 + \frac{1}{N} \|\Delta^a\|^2, \end{aligned} \quad (20)$$

where the summation of the noise terms over Ψ_d is ignored in the large system limit, which again is due to the assumption of $\mathcal{O}(1)$ terms in Ψ_d . Therefore, in the sparse coupling case,

the average RSS defined in (6) can be computed as

$$\mathcal{E} \approx \sum_{j \in \Omega_1} |J_j^* - \bar{J}_j|^2 + \sum_{j \in \Psi_d \setminus \Omega_1} \bar{J}_j^2 + R, \quad (21)$$

where $\Psi_d \setminus \Omega_1$ denotes the truncated set Ψ_d excluding Ω_1 , and a macroscopic parameter R is introduced as

$$R = \frac{1}{N} \sum_{j \in \bar{\Psi}_d} \Delta_j^2, \quad (22)$$

which indicates the sum of square errors in the set $\bar{\Psi}_d$.

3.2 Free Energy Density

Following the sparse ansatz in Section 3.1, the replicated partition function $[Z^n]_{\mathcal{D}M}$ of (15) in the sparse case can be written as

$$\begin{aligned} [Z^n]_{\mathcal{D}M} &= \int \prod_{a=1}^n d\mathbf{J}^a e^{-\lambda\beta N \sum_{a=1}^n \|\mathbf{J}^a\|^2} \left\{ \sum_{\mathbf{s}} P_{\text{Ising}}(\mathbf{s} | \mathbf{J}^*) \exp \left[-\beta \sum_{a=1}^n \Phi(s_0 h^a) \right] \right\}^{\alpha N} \\ &\approx \int \prod_{a=1}^n d\Delta^a e^{-\lambda\beta (Nn \sum_{j \in \Psi_d} \bar{J}_j^2 + \sum_{a=1}^n \|\Delta^a\|^2)} \times \\ &\quad \left\{ \sum_{\mathbf{s}} P_{\text{Ising}}(\mathbf{s} | \mathbf{J}^*) \prod_a \int dh_{\Delta}^a \delta \left(h_{\Delta}^a - \frac{1}{\sqrt{N}} \sum_{j \in \bar{\Psi}_d} \Delta_j^a s_j \right) e^{-\beta \sum_{a=1}^n \Phi(s_0 (\sum_{j \in \Psi_d} \bar{J}_j s_j + h_{\Delta}^a))} \right\}^{\alpha N} \\ &= \int \prod_{a=1}^n d\Delta^a e^{-\lambda\beta (Nn \sum_{j \in \Psi_d} \bar{J}_j^2 + \sum_{a=1}^n \|\Delta^a\|^2)} \times \\ &\quad \left\{ \sum_{s_0, \mathbf{s}_{\Psi_d}} P(s_0, \mathbf{s}_{\Psi_d}, \{h_{\Delta}^a\}_a | \mathbf{J}^*, \{\Delta^a\}_a) e^{-\beta \sum_{a=1}^n \Phi(s_0 (\sum_{j \in \Psi_d} \bar{J}_j s_j + h_{\Delta}^a))} \right\}^{\alpha N} \\ &\approx \int \prod_{a=1}^n d\Delta^a e^{-\lambda\beta (Nn \sum_{j \in \Psi_d} \bar{J}_j^2 + \sum_{a=1}^n \|\Delta^a\|^2)} \times \\ &\quad \left\{ \sum_{s_0, \mathbf{s}_{\Psi_d}} P(s_0, \mathbf{s}_{\Psi_d} | \mathbf{J}^*) \prod_{a=1}^n dh_{\Delta}^a P_{\text{cav}}(\{h_{\Delta}^a\}_a | \{\Delta^a\}_a) e^{-\beta \sum_{a=1}^n \Phi(s_0 (\sum_{j \in \Psi_d} \bar{J}_j s_j + h_{\Delta}^a))} \right\}^{\alpha N}, \end{aligned} \quad (23)$$

where \mathbf{s}_{Ψ_d} is the vector of spins in the truncated set Ψ_d . In the second line of (23), $\sum_{j \in \Psi_d} (\Delta_j^a)^2$ is ignored as in (20), and in the last line, asymptotic uncorrelatedness be-

tween h_Δ^a and s_0, \mathbf{s}_{Ψ_d} is assumed. Please refer to Abbara et al. (2020) for a detailed examination of this assumption. The marginal distribution $\sum_{s_0, \mathbf{s}_{\Psi_d}} P(s_0, \mathbf{s}_{\Psi_d} | J^*)$ is computed by marginalizing the whole distribution $\sum_{\mathbf{s}} P_{\text{Ising}}(\mathbf{s} | J^*)$ with respect to $\mathbf{s}_{\bar{\Psi}_d}$, which can be obtained as

$$P(s_0, \mathbf{s}_{\Psi_d} | J^*) = \sum_{\mathbf{s}_{\bar{\Psi}_d}} P(\mathbf{s} | J^*). \quad (24)$$

Then, according to the central limit theorem, the noise part $\left\{h_\Delta^a\right\}_{a=1}^n$ can be regarded as Gaussian variables so that the cavity distribution $P_{\text{cav}}\left(\left\{h_\Delta^a\right\}_a \mid \left\{\Delta^a\right\}_a\right)$ can be assumed as a multivariate Gaussian distribution. Therefore, two order parameters are introduced:

$$Q \doteq \frac{1}{N} \sum_{i,j \in \bar{\Psi}_d} \Delta_i^a C_{ij}^{\setminus 0} \Delta_j^a, \quad (25)$$

$$q \doteq \frac{1}{N} \sum_{i,j \in \bar{\Psi}_d} \Delta_i^a C_{ij}^{\setminus 0} \Delta_j^b, \quad (a \neq b), \quad (26)$$

where $\mathbf{C}^{\setminus 0} = \left(C_{ij}^{\setminus 0}\right)_{ij}$ is the correlation matrix of the reduced spin system without s_0 . As suggested in Bachschmid-Romano and Opper (2017); Abbara et al. (2020), the non-diagonal elements of $\mathbf{C}^{\setminus 0}$ will have a nontrivial contribution and will hence be retained. To write the integration in terms of the order parameters Q, q , we introduce the following trivial identities:

$$1 = N \int dQ \delta \left(\sum_{i,j \neq 0} \Delta_i^a C_{ij}^{\setminus 0} \Delta_j^a - NQ \right), \quad a = 1, \dots, n, \quad (27)$$

$$1 = N \int dq \delta \left(\sum_{i,j \neq 0} \Delta_i^a C_{ij}^{\setminus 0} \Delta_j^b - Nq \right), \quad a < b, a, b \neq *. \quad (28)$$

Therefore, $[Z^n]_{\mathcal{DM}}$ can be rewritten as

$$\begin{aligned} [Z^n]_{\mathcal{DM}} &= e^{-\lambda \beta N n \sum_{j \in \Psi_d} \bar{J}_j^2} \int dQ dq \int \prod_{a=1}^n d\Delta^a e^{-\lambda \beta \sum_{a=1}^n \|\Delta^a\|^2} \prod_{a=1}^n \delta \left(\sum_{i,j} \Delta_i^a C_{ij}^{\setminus 0} \Delta_j^a - NQ \right) \times \\ &\prod_{a < b} \delta \left(\sum_{i,j} \Delta_i^a C_{ij}^{\setminus 0} \Delta_j^b - Nq \right) \times \end{aligned}$$

$$\begin{aligned}
 & \left\{ \sum_{s_0, \mathbf{s}_{\Psi_d}} P(s_0, \mathbf{s}_{\Psi_d} | J^*) \prod_{a=1}^n dh_{\Delta}^a P_{\text{cav}} \left(\{h_{\Delta}^a\}_a \mid \{\Delta^a\}_a \right) e^{-\beta \sum_{a=1}^n \Phi(s_0(\sum_{j \in \Psi_d} \bar{J}_j s_j + h_{\Delta}^a))} \right\}^{\alpha N} \\
 & = \int dQ dq \exp[NS + M \log L], \tag{29}
 \end{aligned}$$

where

$$\begin{aligned}
 e^{NS} & \doteq e^{-\lambda \beta N n \sum_{j \in \Psi_d} \bar{J}_j^2} \int \prod_{a=1}^n d\Delta^a e^{-\lambda \beta \sum_{a=1}^n \|\Delta^a\|^2} \prod_{a=1}^n \delta \left(\sum_{i,j} \Delta_i^a C_{ij}^{\setminus 0} \Delta_j^a - NQ \right) \\
 & \quad \times \prod_{a < b} \delta \left(\sum_{i,j} \Delta_i^a C_{ij}^{\setminus 0} \Delta_j^b - Nq \right), \tag{30}
 \end{aligned}$$

$$L \doteq \sum_{s_0, \mathbf{s}_{\Psi_d}} P(s_0, \mathbf{s}_{\Psi_d} | J^*) \int \prod_{a=1}^n dh_{\Delta}^a P_{\text{cav}} \left(\{h_{\Delta}^a\}_a \mid \{\Delta^a\}_a \right) e^{-\beta \sum_{a=1}^n \Phi(s_0(\sum_{j \in \Psi_d} \bar{J}_j s_j + h_{\Delta}^a))}. \tag{31}$$

After performing some algebraic operations presented in Appendix A and Appendix B, we obtain the results in the limit $n \rightarrow 0$:

$$\begin{aligned}
 \lim_{n \rightarrow 0} \frac{S}{n} & = -\lambda \beta \sum_{j \in \Psi_d} \bar{J}_j^2 + \frac{Q\beta}{2} G_1^{-1}(\beta(Q-q)) - \frac{1}{2} G_2(G_1^{-1}(\beta(Q-q))) \\
 & \quad + \frac{1}{2} \log \frac{2\pi}{\beta} - \frac{1}{2N} \text{Tr} \log (\mathbf{C}^{\setminus 0})^{-1}, \tag{32}
 \end{aligned}$$

$$\lim_{n \rightarrow 0} \frac{1}{n} \log L = \sum_{s_0, \mathbf{s}_{\Psi_d}} P(s_0, \mathbf{s}_{\Psi_d} | J^*) \int \mathcal{D}z \log \int \mathcal{D}v e^{-\beta \sum_{a=1}^n \Phi(s_0(\sum_{j \in \Psi_d} \bar{J}_j s_j + \sqrt{Q-q}v + \sqrt{q}z))}, \tag{33}$$

where $\mathcal{D}z = \frac{dz}{\sqrt{2\pi}} e^{-\frac{z^2}{2}}$, and

$$G_1(x) = \int \frac{d\eta \rho(\eta)}{x + 2\lambda\eta}, \tag{34}$$

$$G_2(x) = \int d\eta \rho(\eta) \log(x + 2\lambda\eta), \tag{35}$$

where $\rho(\eta)$ is the eigenvalue distribution (EVD) of the inverse correlation matrix, i.e., $(\mathbf{C}^{\setminus 0})^{-1}$, as shown in Appendix E. Note that G_1^{-1} denotes the inverse function of G_1 , i.e.,

$x = G_1^{-1}(y)$ implies that $y = G_1(x)$. In the special case of $\lambda = 0$, $G_1(x) = 1/x$ and $G_1^{-1}(y) = 1/y$.

Further, we take the limit $\beta \rightarrow \infty$, which requires the following relation (Bachschmid-Romano and Opper, 2017; Abbara et al., 2020):

$$\lim_{\beta \rightarrow \infty} \beta(Q - q) = \chi = \mathcal{O}(1). \quad (36)$$

$\chi = \mathcal{O}(1)$ is a finite number, and according to (34), $G_1^{-1}(\beta(Q - q))$ should also be a finite number. Then, denoting $G_1^{-1}(\beta(Q - q)) \doteq \kappa$, after performing some algebraic operations, we obtain the free energy density (14) in the limit $\beta \rightarrow \infty$ as

$$f(\beta \rightarrow \infty) = -\text{Extr}_{Q, \kappa} \left\{ -\lambda \sum_{j \in \Psi_d} \bar{J}_j^2 + \frac{Q}{2} \kappa + \alpha \sum_{s_0, \mathbf{s}_{\Psi_d}} P(s_0, \mathbf{s}_{\Psi_d} | J^*) \int \mathcal{D}z \max_y \left[-\frac{\left(y - s_0 \left(\sqrt{Q}z + \sum_{j \in \Psi_d} \bar{J}_j s_j \right) \right)^2}{2G_1(\kappa)} - \Phi(y) \right] \right\}, \quad (37)$$

where $\text{Extr}_x \{\cdot\}$ denotes extremization w.r.t. x .

3.3 Equations of State (EOS)

Consequently, from (37), the extremization condition leads to the following equations of state (EOS):

$$\kappa - \frac{\alpha}{\sqrt{Q}} \int \mathcal{D}z z \frac{\partial l(y)}{\partial y} \Big|_{y=\hat{y}} = 0, \quad (38)$$

$$Q + \alpha G_1'(\kappa) \int \mathcal{D}z \left(\frac{\partial l(y)}{\partial y} \Big|_{y=\hat{y}} \right)^2 = 0, \quad (39)$$

where

$$\hat{y} = \arg \max_y \left(-\frac{\left(y - s_0 \left(\sqrt{Q}z + \sum_{j \in \Psi_d} \bar{J}_j s_j \right) \right)^2}{2G_1(\kappa)} - \Phi(y) \right). \quad (40)$$

Moreover, the mean estimates $\{\bar{J}_j\}_{j \in \Psi_d}$ can also be evaluated by the extremization condition, i.e.,

$$0 = 2\lambda\bar{J}_j + \alpha \sum_{s_0, \mathbf{s}_{\Psi_d}} P(s_0, \mathbf{s}_{\Psi_d} | J^*) \int \mathcal{D}z \frac{\partial \Phi(y)}{\partial y} \Big|_{y=\hat{y}} s_0 s_j, \quad j \in \Psi_d, \quad (41)$$

which is a set of linear equations in our case of the quadratic cost function. Note that when the coupling strength is uniform, i.e., $|J_j^*| = K$, $j \in \Omega_1$, the strength of the mean estimates $\bar{J}_j \in \Omega_1$ can also be set to a uniform value $|\bar{J}_j| = \bar{K} = \hat{b}K$, where the bias factor is defined as

$$\hat{b} \doteq \frac{\bar{K}}{K}. \quad (42)$$

The bias factor \hat{b} can be directly computed using the mean estimates $\bar{J}_j \in \Omega_1$. Moreover, using the auxiliary variable technique similar to Abbara et al. (2020), as shown in Appendix C, the macroscopic parameter R in (22) can be computed as

$$R = \frac{1}{N} \sum_{j \in \bar{\Psi}_d} \Delta_j^2 = q \frac{G_3'(\kappa)}{G_1'(\kappa)}, \quad (43)$$

where

$$G_3(x) = \int \frac{d\eta \rho(\eta) \eta}{(x + 2\lambda\eta)}, \quad (44)$$

and $G_1'(x)$ and $G_3'(x)$ are the first-order derivatives of $G_1(x)$ and $G_3(x)$, respectively. Then, given $\{\bar{J}_j\}_{j \in \Psi_d}$, Q , κ , the RSS in (6) can be computed as

$$\mathcal{E} \approx \sum_{j \in \Omega_1} |J_j^* - \bar{J}_j|^2 + \sum_{j \in \Psi_d \setminus \Omega_1} \bar{J}_j^2 + Q \frac{G_3'(\kappa)}{G_1'(\kappa)}. \quad (45)$$

In general, no analytical solution exists for RSS, but it can be easily solved using numerical methods, as illustrated in Appendix D.

3.4 Nearest-Neighbor Effect

In this subsection, we study the nearest-neighbor (NN) effect by examining the estimates $\{\bar{J}_j\}_{j \in \Psi_d}$, based on which the application range of ansatz (16) is also discussed. According to the replica analysis presented above, the estimates $\{\bar{J}_j\}_{j \in \Psi_d}$ can be calculated from (41) by solving the linear equations

$$(1 + 2\lambda/\kappa) \bar{J}_j + \sum_{i \in \Psi_d, i \neq j} \bar{J}_i \langle s_i s_j \rangle - \langle s_0 s_j \rangle = 0, \quad j \in \Psi_d, \quad (46)$$

where $\langle s_i s_j \rangle$ is the correlation function w.r.t. the joint distribution $P(s_0, \mathbf{s}_{\Psi_d} | J^*)$. First, consider the special case without regularization. The result is given in Theorem 1.

Theorem 1 *For a sparse tree-like graph under a paramagnet assumption (Oppen and Saad, 2001; Mezard and Montanari, 2009), using linear regression without regularization, i.e., $\lambda = 0$, the mean estimates $\{\bar{J}_j\}_{j \in \Psi_d}$ in (46) are*

$$\bar{J}_j = \begin{cases} \frac{1}{\sum_{k \in \Omega_1} \frac{1}{1 - \tanh^2 J_k^*} - c + 1} \cdot \frac{\tanh(J_j^*)}{1 - \tanh^2(J_j^*)} & j \in \Omega_1 \\ 0, & j \notin \Omega_1 \end{cases}, \quad (47)$$

where c is the number of first-generation nearest neighbors of s_0 , i.e., $c = |\Omega_1|$. In particular, with uniform coupling, i.e., $|J_j^*| = K, j \in \Omega_1$, it is

$$\bar{J}_j = \begin{cases} \frac{\tanh K}{1 + (c-1) \tanh^2 K} \text{sign}(J_j^*), & j \in \Omega_1 \\ 0, & j \notin \Omega_1 \end{cases}. \quad (48)$$

The proof is given in Appendix F. Theorem 1 shows that, even under model mismatch, naive linear regression without regularization can reconstruct the active set Ω_1 , i.e., $\bar{J}_j = 0, j \in \Psi_d \setminus \Omega_1$. This result is consistent with the result in Abbara et al. (2020), which is obtained by analyzing the zero-gradient condition for the general loss function. Consequently, when $\lambda = 0$, we can simply ignore the biases $\bar{J}_j, j \notin \Omega_1$ of the estimator when computing the RSS in (45).

However, when there is regularization, i.e., $\lambda > 0$, the result is different, as shown in Theorem 2.

Theorem 2 *For a sparse tree-like graph under a paramagnet assumption (Oppen and Saad, 2001; Mezard and Montanari, 2009), with uniform coupling strength K , using ℓ_2 -regularized linear regression with regularization coefficient $\lambda > 0$, the mean estimates $\{\bar{J}_j\}_{j \in \Psi_d}$ in (46) are biased to nonzero values in the inactive set but decay at least exponentially fast w.r.t. the distance from spin s_0 with factor $\delta = \theta \frac{(D-1)}{D-\theta^2}$, where $D = 1 + \frac{2\lambda}{\kappa}$ and $\theta = \tanh K$.*

The proof is given in Appendix G. Theorem 2 shows that the use of ℓ_2 regularization in ridge regression introduces biases into the coupling estimates for the inactive set; hence, one must be careful about the potential false positives when using ℓ_2 regularization. The biases decay at least exponentially fast w.r.t. the distance d between s_j and s_0 , i.e., $|\bar{J}_j / \bar{J}_k| < \delta^{d-1}, j \in \Omega_d, k \in \Omega_1$. Thus, despite the nonzero biases in the inactive set, the ansatz (16) is still applicable if we consider only a truncated NN set $\Psi_d = \{\Omega_1, \Omega_2, \dots, \Omega_d\}$ up to a finite distance $d = \mathcal{O}(1)$. This result holds for a tree graph and will also apply if the graph is asymptotically tree-like in the large system limit. However, if there is a loop in the graph, further analysis and modifications are required. Specifically, for a random regular

(RR) graph with uniform coupling strength K , the total contribution of the d -th generation spins in Ω_d from spin s_0 to the average RSS \mathcal{E} satisfies

$$\text{RSS}_{\Omega_d} < c(c-1)^{d-1} [\tanh^2(K)]^{d-1} \bar{J}_{\Omega_1}, \quad (49)$$

where \bar{J}_{Ω_1} is the estimate of the mean coupling strength in the active set Ω_1 . Thus, from (49), as long as $(c-1)\tanh^2 K < 1$, the contribution RSS_{Ω_d} of the NN spins with distance d can be safely ignored when d is large enough. Interestingly, the paramagnetic condition $(c-1)\tanh^2 K < 1$ (Oppen and Saad, 2001; Mezard and Montanari, 2009) corresponds to the converging condition of RSS_{Ω_d} as d increases.

4. Structure Learning via Two-Stage Estimator

To reconstruct the topology structure of the original teacher network, one must infer the presence/absence of teacher couplings based on the estimator $\hat{\mathbf{J}}$. From the statistical mechanics analysis presented in Section 3, for naive linear regression without regularization, the estimates in the inactive set $\hat{J}_j \sim \mathcal{O}(1/\sqrt{N})$, $j \notin \Omega_1$ are unbiased; hence, it is expected that $\hat{J}_j \rightarrow 0$, $j \notin \Omega_1$ in the large system limit. Consequently, perfect recovery of the graph structure of the teacher network is possible by choosing a proper threshold \bar{J}_{th} , similarly to Abbara et al. (2020). However, this is possible only when $\alpha > 1$, as signaled by the divergent RSS in the limit $\alpha \rightarrow 1$, as illustrated in Section 5. This severely limits the applicability in situations when the number of observations is smaller than the number of Ising spins, which is typical in practical applications. Owing to the use of ℓ_2 regularization in ridge regression, the problem of divergence in $\alpha \rightarrow 1$ is overcome as long as the regularization coefficient $\lambda > 0$. However, as shown in Theorem 2, the use of ℓ_2 regularization leads to biased estimates in the inactive set; hence, one must carefully choose a certain threshold to avoid the potential false positives, which is difficult. Nevertheless, the biases decay at least exponentially fast w.r.t. the distance. Inspired by this observation, we propose a two-stage linear estimator, which combines the advantages of both naive linear regression and ℓ_2 -regularized linear regression.

Specifically, in the first stage, ℓ_2 -regularized linear regression is applied and the resultant estimate of couplings is denoted as $\hat{\mathbf{J}}^{\text{stg1}}$. To control false positives, a certain constant threshold value $K_1 (\sim \mathcal{O}(1))$ is introduced, and the elements of $\hat{\mathbf{J}}^{\text{stg1}}$ whose absolute values are less than K_1 are considered as negligible and set to zero, i.e.,

$$\hat{J}_j^{\text{stg1-th}} = \begin{cases} \hat{J}_j^{\text{stg1}} & \text{if } |\hat{J}_j^{\text{stg1}}| > K_1, \\ 0 & \text{otherwise.} \end{cases} \quad (50)$$

Compared with the single-step estimator, the threshold K_1 is not necessarily required to eliminate all the false positives, but it should be sufficiently small to avoid false negatives, which is relatively easy to implement, as demonstrated in Section 5. According to Theorem

2, the biases in the inactive set decay exponentially fast; hence, there will be only $\mathcal{O}(1)$ false positives in $\hat{\mathbf{J}}^{\text{stg1-th}}$. To further eliminate the $\mathcal{O}(1)$ false positives, in the second stage, linear regression without regularization is applied only to the support of $\hat{\mathbf{J}}^{\text{stg1-th}}$, which leads to the estimation $\hat{\mathbf{J}}^{\text{stg2}}$. Since there are only $\mathcal{O}(1)$ false positives after the first stage, the problem in the second stage corresponds to the situation $\alpha \rightarrow \infty$ ($\mathcal{O}(1)$ unknowns but with $M \rightarrow \infty$ samples) in the large system limit; hence, perfect reconstruction will be guaranteed by Theorem 1. Therefore, the two-stage method can achieve perfect recovery of the presence/absence of couplings in the teacher network. In practice, owing to the finite effect, a post-threshold is required after stage two, i.e., a certain constant threshold value $K_2(\sim \mathcal{O}(1))$ is chosen so that all $|\hat{J}_j^{\text{stg2}}| < K_2$ are declared to be zero. This result supports the underlying possibility of perfect structure learning for inverse Ising problems with a quantitatively satisfactory performance even in the presence of model mismatch.

5. Numerical experiments

This section describes numerical experiments conducted to verify the accuracy of the theoretical analysis and the validity of the simple linear estimator in structure learning in inverse Ising problems. We use the random regular (RR) graph and the Erdős–Rényi (ER) graph as representative examples of sparse tree-like graphs. The RR graph is characterized by a connectivity parameter c and uniform coupling strength K while, the ER graph is characterized by the connection probability p . As in Abbara et al. (2020), to keep the generated graph sufficiently sparse in the ER case, the probability p is assumed to scale as $p = \bar{c}/N$, yielding the mean degree \bar{c} . We assume that the active couplings of the teacher model have the same probability of taking both signs with strength $|J_i^*| = K, i \in \Omega_1$. In addition, for both RR and ER graphs, K is assumed to be sufficiently small to satisfy the paramagnet assumption of the teacher model (Opper and Saad, 2001; Mezard and Montanari, 2009). The experimental procedures are similar to those in Abbara et al. (2020). First, a random graph for the teacher system with sparse couplings is generated, from which the spin snapshots are obtained using MC sampling. Then, we randomly choose a center spin s_0 from all the spins and infer the associated couplings connected to s_0 by applying the PL method to the sampled training dataset \mathcal{D}^M . The experimental values of the macroscopic quantities of interest, such as RSS, can be easily obtained by standard linear algebra. To obtain the error bars of these estimates, we repeat the sequence of operations many times. Note that in the MC sampling, we started from a random initial configuration and updated the state by the standard Metropolis method; one MC step (MCS) is defined by N trial flips of spins, where N is the total number of spins. We discarded the first 10^5 MCSs as burn-in to avoid systematic errors from the initialization. Furthermore, to avoid possible correlations in the samples, each dataset for learning was generated by subsampling from a much larger dataset, which consists of all the configurations recorded after every few MCSs.

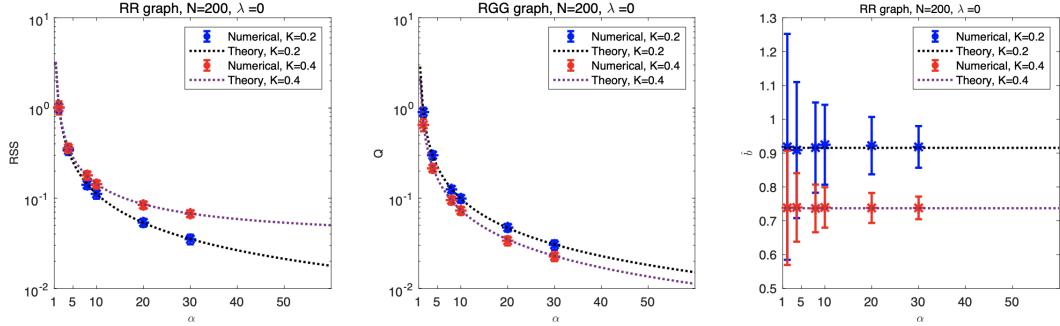


Figure 2: Plots of RSS \mathcal{E} , Q , and bias factor \hat{b} for the RR graph with $(N, c) = (200, 3)$ for $K = 0.2, 0.4$ using linear regression, i.e., $\lambda = 0$. The dotted lines and colored markers represent the replica prediction and numerical values, respectively. The RSS and Q diverge in the limit $\alpha \rightarrow 1$. The error bars are obtained from 100 random runs.

First, let us consider the PL method using naive linear regression without regularization, i.e., $\lambda = 0$. In this case, the truncated NN set Ψ_d is set to be $\Psi_d = \Omega_1$ in the theoretical analysis, as the estimates are unbiased in the inactive set as stated in Theorem 1. The theoretical and experimental values of the RSS \mathcal{E} , order parameter Q , and bias factor \hat{b} for the RR graph are shown in Fig. 2, where the error bars are obtained from 100 random runs. As can be seen from Fig. 2, the experimental results and theoretical results are in fairly good agreement, which supports the validity of the theoretical analysis. For structure learning, Fig. 3 shows the empirical recall rate and precision rate using naive linear regression for both the RR graph and the ER graph when $\alpha = 10$ (results with other values $\alpha > 1$ are similar). Despite the model mismatch in the naive linear regression, perfect structure recovery, i.e., both recall rate and precision rate equal to 1, is possible with a properly chosen threshold. As N increases, the optimal threshold interval that corresponds to perfect structure recovery becomes larger, and in the large system limit, it approaches $(0, \bar{J}_{\text{th}})$, where $\bar{J}_{\text{th}} = \min_{j \in \Omega_1} |\bar{J}_j|$ is the minimum mean estimate of couplings in the active set Ω_1 . However, as shown in Fig. 2, the result of linear regression is not informative in the region $\alpha \leq 1$ because the RSS and Q will diverge in the limit $\alpha \rightarrow 1$. This implies that, by using naive linear regression without regularization, perfect identification of the network topology is possible only when the dataset size M is greater than the number of Ising spins N .

Next, we consider the PL method using ℓ_2 -regularized linear regression (ridge regression). The theoretical and experimental values of the RSS \mathcal{E} , order parameter Q , and bias factor \hat{b} for the RR graph are shown in Fig. 4. Compared to Fig. 2 for naive linear regression,

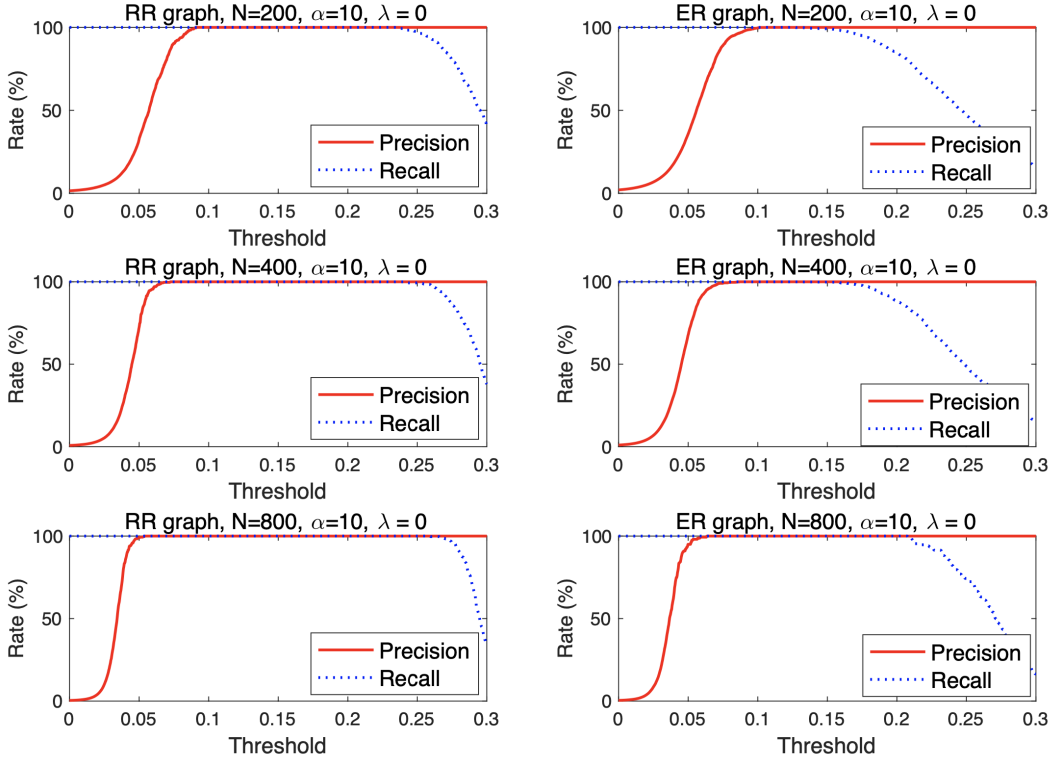


Figure 3: Precision and recall rate for RR and ER graphs using naive linear regression without regularization for different N in the case of $K = 0.4$ and $\alpha = 10$. For the RR graph, $c = 3$; for the ER graph, $\bar{c} = 4$. The dotted and solid lines represent the recall and precision rates, respectively. Ten different ER graphs are generated, each with two independent MC samplings, and learning is then conducted for all $i = 0, \dots, N - 1$.

there are three main differences for the ℓ_2 -regularized linear estimator. First, the use of ℓ_2 regularization successfully eliminates the problem of divergence in the limit $\alpha \rightarrow 1$, making it applicable in the region $\alpha < 1$, which is highly desirable when the dataset size M is smaller than the number of Ising spins N . Second, the biases of the neighboring spins cannot always be ignored, especially when λ and/or K is large, as indicated by the lower part of Fig. 4, which shows the apparent discrepancy between the experimental results and the theoretical prediction when ignoring all the biases $\{\bar{J}_j\}_{j \in \Omega_d, d \geq 2}$. This implies that one must be very careful about the potential false positives caused by the nonzero biases of the $d \geq 2$ neighboring spins when using ℓ_2 -regularized linear regression. This is consistent with the result in Theorem 2: when λ and/or K is large, the decay factor $\delta = \theta \frac{(D-1)}{D-\theta^2}$ is high; hence, the biases in the inactive set decay slowly. Owing to the exponential decay, it is

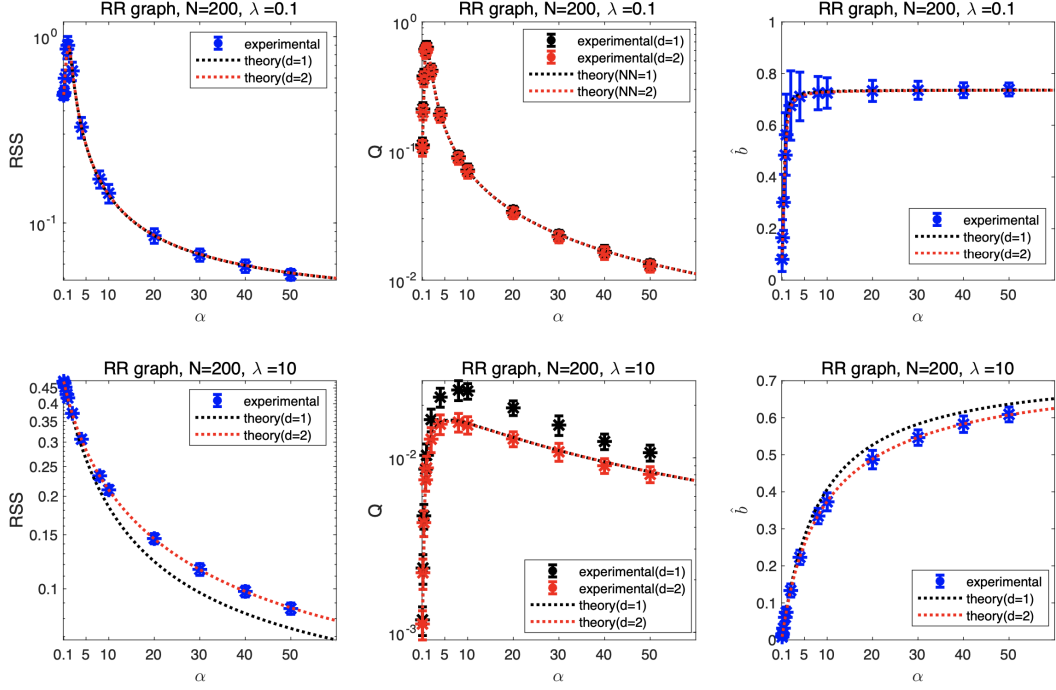


Figure 4: Plots of RSS \mathcal{E} , Q , and bias factor \hat{b} for the RR graph with $(N, c) = (200, 3)$ with $K = 0.4$ using ridge regression with $\lambda = 0.1, 10$. The dotted lines and colored markers represent the replica prediction and numerical values, respectively. Note that the experimental values of Q are different for $d = 1$ and $d = 2$ since Q is related to the definition of Ψ_d , as shown in (25). The error bars are obtained from 100 random runs.

sufficient to consider only a truncated NN set $\Psi_d = \{\Omega_1, \Omega_2, \dots, \Omega_d\}$ up to a finite distance $d = \mathcal{O}(1)$. For example, as shown in Fig. 4, considering a truncated set Ψ_d with $d = 2$ leads to fairly good agreement between the theoretical and experimental results. This can also be verified by empirically evaluating the distribution of estimates $\{\hat{J}_j\}$ in different Ω_d , which is shown in Fig. 5 for the first three NN spins. In the lower part of Fig. 5, when the regularization coefficient is $\lambda = 10$, the histograms of the inactive couplings in Ω_d with $d = 2$ are far from the zero-mean Gaussian. Therefore, in this case, apart from the true active set Ω_1 , the NN spins in Ω_2 should also be considered as indicated in Fig. 4. The dashed straight line represents the mean value estimates $\{\bar{J}_j\}$ with different distances d from s_0 computed from (41). When the regularization coefficient is small, e.g., $\lambda = 0.1$, the histograms of inactive couplings in Ω_d , $d \geq 2$ are similar to the zero-mean Gaussian; see the upper part of Fig. 5. In this case, ignoring the spins with $d \geq 2$ in the theoretical analysis still leads to good agreement with the experimental result, which is consistent with

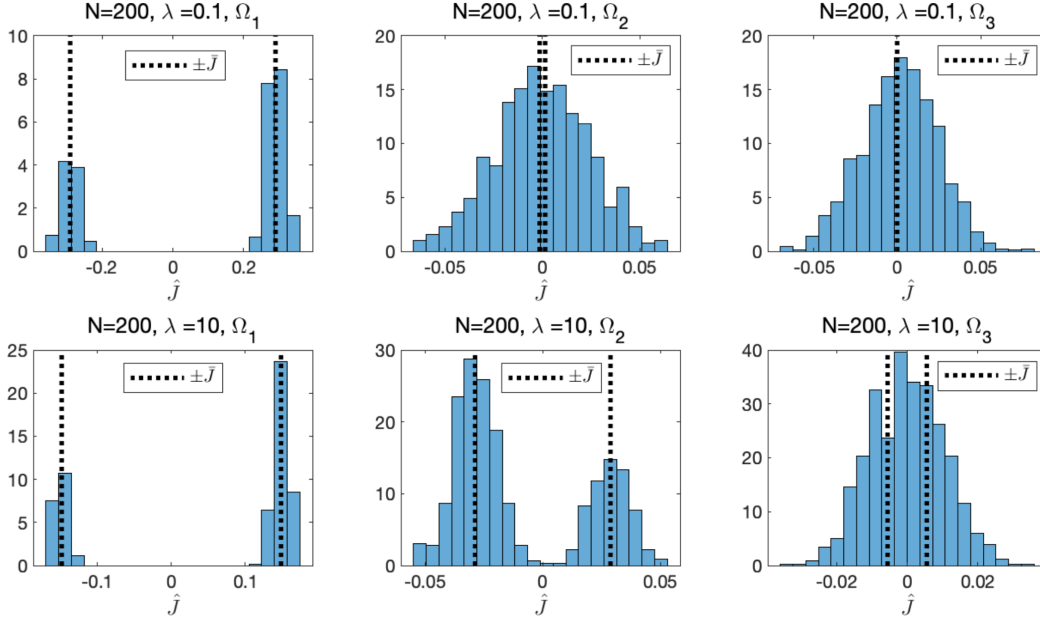


Figure 5: Histograms of the estimations \hat{J} in the first three NN spins set Ω_d , $d = 1, 2, 3$ from s_0 . The system parameters are $(N, K, c, \alpha) = (200, 400, 3, 10)$ with $\lambda = 0.1, 10$. The histograms are generated from 100 random runs. In contrast to linear regression, there are nonzero biases in the NN inactive spins $\Omega_d, d \geq 2$, which cannot always be ignored, especially when λ and/or K is large, e.g., the histograms of the inactive couplings in Ω_2 are far from the zero-mean Gaussian when $\lambda = 10$, as shown in the lower part.

the result in Fig. 4. The last difference between ℓ_2 -regularized linear regression and naive linear regression is that the bias factor \hat{b} is not a constant; it increases as α increases and λ decreases.

Finally, the effectiveness of the proposed two-stage linear estimator for structure learning is evaluated in the case of the RR and ER graphs. Fig. 6 shows a typical result of the empirical precision rate and recall rate for the RR graph using the two-stage linear estimator with different N when $K = 0.4$, $\alpha = 0.8$, $\lambda = 0.1$. Perfect structure recovery can be achieved with a properly chosen threshold as N increases, e.g., $N = 800$ in Fig. 6, which verifies the analysis in Section 4. It is worth noting that, since the noise variance of the estimators in the inactive set scales as $\mathcal{O}(1/N)$, the number of components beyond a certain threshold decreases as N increases, as shown in Fig. 7. This means that as long as the threshold $K_1 \sim \mathcal{O}(1)$ is chosen to be sufficiently small to avoid ignoring true positives, the number

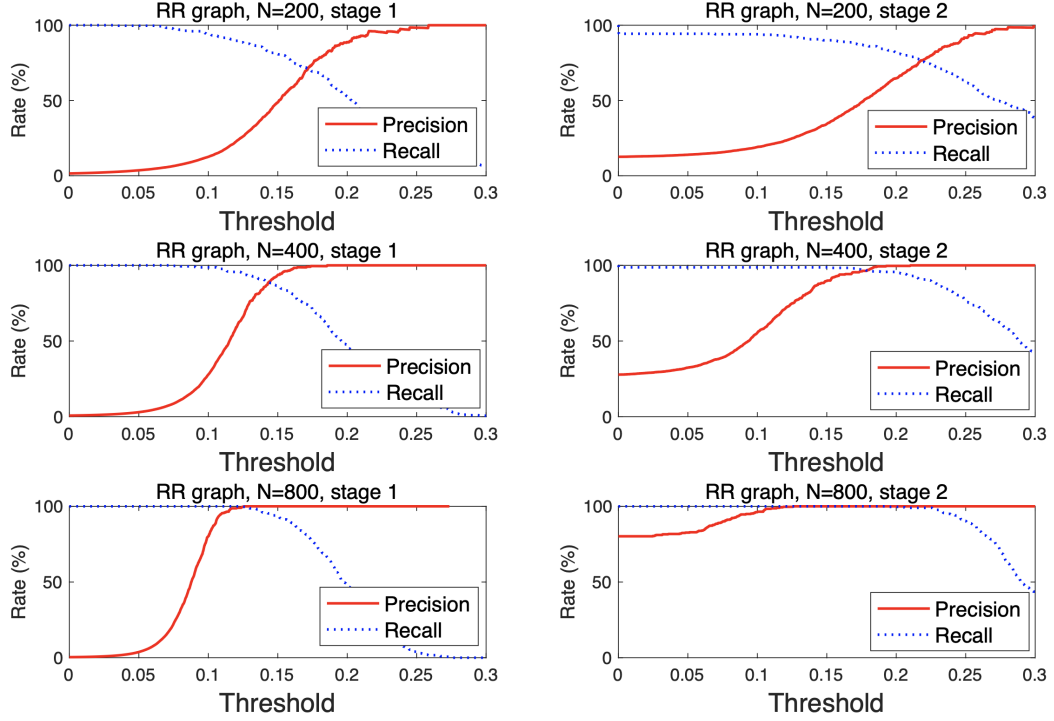


Figure 6: Precision and recall rate for the RR graph using the two-stage estimator for different N in the case of $K = 0.4$, $\lambda = 0.1$, and $\alpha = 0.8$. The dotted and solid lines represent the recall and precision rates, respectively. The threshold after the first stage is set to $K_1 = 0.1$. The results are obtained from 100 random runs.

of false positives after the first stage can be reduced to a certain $\mathcal{O}(1)$ value as $N \rightarrow \infty$. This effectively yields the asymptotic limit of $M \rightarrow \infty$ keeping $N \mathcal{O}(1)$; thus, one can easily distinguish true positives from false positives in the second stage. The validity of the two-stage linear estimator is also evaluated in the case of the ER graph with mean degree $\bar{c} = 4$ when $K = 0.4$, $\alpha = 0.9$, $\lambda = 0.1$, as shown in Fig. 8. Although exact perfect recovery is not achieved (when $N = 1600$, there is a threshold interval where both 99.90% empirical recall rate and 99.90% empirical precision rate can be simultaneously achieved.) owing to the finite size effect, the empirical result in Fig. 8 indicates the tendency of improvement as N increases, which implies perfect recovery for $N \rightarrow \infty$. Note that in the case of the ER graph, we generated 10 different graphs, each with two independent MC samplings, and then conducted learning for all $i = 0, \dots, N - 1$.

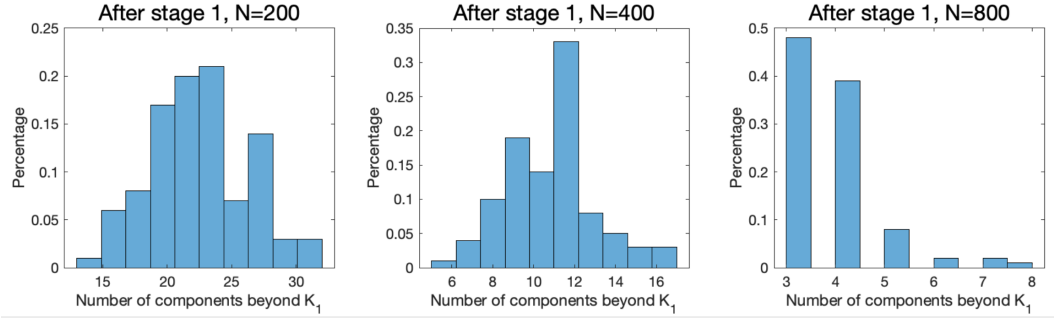


Figure 7: Histogram of the number of components selected after the first stage in the two-stage linear estimator for RR graph of different N in the case of $K = 0.4$, $\lambda = 0.1$, and $\alpha = 0.8$. For a fixed threshold $K_1 = 0.1$, as N increases, the number of components beyond the threshold K_1 decreases as the noise variance scales as $\mathcal{O}(1/N)$. The results are obtained from 100 random runs.

6. Summary and Discussion

We evaluated the utility of the pseudolikelihood (PL) method for inverse Ising problems in the model mismatch case by investigating the inference (learning) performance of the ℓ_2 -regularized linear regression (ridge regression) estimator in the teacher-student scenario, where the couplings of the teacher network are assumed to be sparse and the student has no prior knowledge of its structure and associated parameters. Using the replica and cavity methods of statistical mechanics, we showed that despite the model mismatch, one can perfectly reconstruct the network topology. This is naturally realized owing to the unbiasedness of the linear estimator in the inactive set without regularization, while it is efficiently achieved using the proposed two-stage estimator with regularization, even though the dataset size is smaller than the number of Ising spins. The results of experiments conducted on locally tree-like graphs, such as the random regular (RR) graph and the Erdős–Rényi (ER) graph, verified the validity of both the theoretical analysis and the linear estimator in structure learning in inverse Ising problems.

As with Abbara et al. (2020), the two critical assumptions in this study are the sparse ansatz (16) and the paramagnetic assumption of the teacher network. As discussed in Section 3.1, the sparse ansatz holds for trees and asymptotic tree-like graphs. The paramagnetic assumption implies that the coupling strength should be sufficiently small. Thus, the results in this paper do not apply to strongly correlated datasets in the non-paramagnetic case, which is an important direction for future research. Furthermore, for datasets with possible loop structures, the sparse ansatz (16) should be modified, although the result presented in this paper can serve as an approximation for cases with loop structures. Therefore, another future direction is to evaluate the performance of the proposed method for datasets generated via teacher networks with loopy graphs, e.g., square lattices.

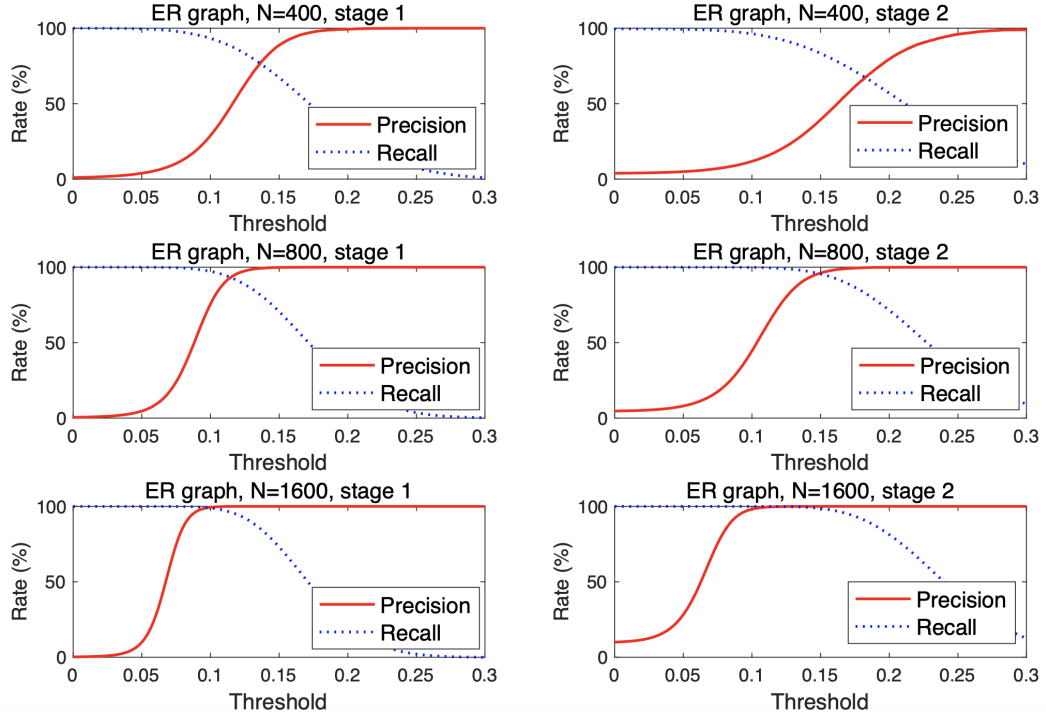


Figure 8: Precision and recall rate for the ER graph using the two-stage estimator for different N in the case of $K = 0.4$, $\lambda = 0.1$, $\bar{c} = 4$, and $\alpha = 0.9$. The dotted and solid lines represent the recall and precision rates, respectively. The threshold after the first stage is set to $K_1 = 0.05$. Owing to the finite size effect, exact perfect recovery is still not achieved when $N = 1600$ (99.90% empirical recall rate and 99.90% empirical precision rate can be achieved simultaneously) but it indicates the tendency of improvement as N increases, implying perfect recovery for $N \rightarrow \infty$. Ten different ER graphs are generated, each with two independent MC samplings, and learning is then conducted for all $i = 0, \dots, N - 1$.

As shown in Section 3.4, the use of ℓ_2 regularization introduces a nonzero bias for spins in the inactive set, which is undesirable although the biases decay exponentially fast. In the case of sparse inference, ℓ_1 regularization is more popular and has been studied for the inverse Ising problem in the model match case (Ravikumar et al., 2010; Santhanam and Wainwright, 2012; Aurell and Ekeberg, 2012; Decelle and Ricci-Tersenghi, 2014; Bresler, 2015). It would be interesting to extend the present analysis of the PL approach to the ℓ_1 -regularized linear estimator (lasso regression) (Tibshirani, 1996) in the model mismatch case within the statistical mechanics framework.

In summary, we presented a statistical mechanics analysis of the inference (learning) performance of the PL method for inverse Ising problems in the model mismatch case. Thus, we provided a theoretical basis for the applicability of the inverse Ising model to real-world datasets whose underlying generating mechanism is usually unknown. Although this model is relatively simple, it can help enhance the theoretical understanding of the general learning process in more complex models.

Acknowledgments

This work was supported by JSPS KAKENHI Nos. 17H00764, 18K11463, and 19H01812, and JST CREST Grant Number JPMJCR1912, Japan.

Appendices

Appendix A Computation of e^{NS}

According to the definition in (30), we have

$$\begin{aligned}
 e^{NS} &= e^{-\lambda\beta Nn \sum_{j \in \Psi_d} \bar{J}_j^2} \int \prod_{a=1}^n d\Delta^a e^{-\lambda\beta \sum_{a=1}^n \|\Delta^a\|^2} \prod_{a=1}^n \delta \left(\sum_{i,j} \Delta_i^a C_{ij}^{\setminus 0} \Delta_j^a - NQ \right) \\
 &\quad \times \prod_{a < b} \delta \left(\sum_{i,j} \Delta_i^a C_{ij}^{\setminus 0} \Delta_j^b - Nq \right). \tag{51}
 \end{aligned}$$

The non-diagonality of $\mathbf{C}^{\setminus 0} = \{C_{ij}^{\setminus 0}\}$ will complicate subsequent computations; hence, we first diagonalize it by introducing an orthogonal matrix U such that $\mathbf{C}^{\setminus 0} = U^T \Lambda U$, where $\Lambda = \text{diag}[\gamma_1, \dots, \gamma_{N-1}]$. Consequently, the term $\sum_{i,j} W_i^a C_{ij}^{\setminus 0} W_j^*$ becomes

$$\begin{aligned}
 \sum_{i,j} \Delta_i^a C_{ij}^{\setminus 0} \Delta_j^a &= (\Delta^a)^T \mathbf{C}^{\setminus 0} \Delta^a \\
 &= (\Delta^a)^T U^T \Lambda U \Delta^a \\
 &= (U \Delta^a)^T \Lambda (U \Delta^a) \\
 &= (\tilde{\Delta}^a)^T \Lambda \tilde{\Delta}^a, \tag{52}
 \end{aligned}$$

where $\tilde{\Delta}^a = U \Delta^a$. Similarly, $\sum_{i,j} \Delta_i^a C_{ij}^{\setminus 0} \Delta_j^b = (\tilde{\Delta}^a)^T \Lambda \tilde{\Delta}^b$, and $\|\tilde{\Delta}^a\|^2 = \|\Delta^a\|^2$. By performing the variable transformation in (51), we obtain

$$e^{NS} \doteq e^{-\lambda\beta Nn \sum_{j \in \Psi_d} \bar{J}_j^2} \int \prod_{a=1}^n d\Delta^a e^{-\lambda\beta \sum_{a=1}^n \|\Delta^a\|^2} \\ \times \prod_{a=1}^n \delta \left(\sum_{i,j} \Delta_i^a C_{ij}^{\setminus 0} \Delta_j^a - NQ \right) \prod_{a < b} \delta \left(\sum_{i,j} \Delta_i^a C_{ij}^{\setminus 0} \Delta_j^b - Nq \right). \quad (53)$$

Then, the delta functions can be expressed as integrals over auxiliary parameters using the Fourier transform of the delta function, i.e.,

$$\begin{cases} \delta \left(\sum_{i,j} \Delta_i^a C_{ij}^{\setminus 0} \Delta_j^a - NQ \right) = \int d\hat{Q} e^{\hat{Q} \left(\sum_{i,j} \Delta_i^a C_{ij}^{\setminus 0} \Delta_j^a - NQ \right)}, \\ \delta \left(\sum_{i,j} \Delta_i^a C_{ij}^{\setminus 0} \Delta_j^b - Nq \right) = \int d\hat{q} e^{\hat{q} \left(\sum_{i,j} \Delta_i^a C_{ij}^{\setminus 0} \Delta_j^b - Nq \right)}, \end{cases} \quad (54)$$

where the integration over \hat{Q}, \hat{q} is on the imaginary axis. Hence, (53) can be rewritten as

$$e^{NS} = \int d\hat{Q} d\hat{q} e^{-N \left(n\hat{Q}Q + \frac{n(n-1)}{2} \hat{q}q \right)} e^{-\lambda\beta Nn \sum_{j \in \Psi_d} \bar{J}_j^2} \int \prod_{a=1}^n d\Delta^a e^{-\lambda\beta \sum_{a=1}^n \|\Delta^a\|^2} \\ \times \exp \left\{ \hat{Q} \sum_a (\Delta^a)^T \Lambda \Delta^a + \hat{q} \sum_{a < b} (\Delta^a)^T \Lambda \Delta^b \right\}, \\ = \int d\hat{Q} d\hat{q} e^{-N \left(n\hat{Q}Q + \frac{n(n-1)}{2} \hat{q}q \right)} e^{-\lambda\beta N \sum_{j \in \Psi_d} \bar{J}_j^2} \int \prod_{a=1}^n d\Delta^a e^{-\lambda\beta \sum_{a=1}^n \|\Delta^a\|^2} \\ \times \exp \left\{ \left(\hat{Q} - \frac{\hat{q}}{2} \right) \sum_a (\Delta^a)^T \Lambda \Delta^a + \frac{\hat{q}}{2} \sum_{a,b} (\Delta^a)^T \Lambda \Delta^b \right\}, \\ = \int d\hat{Q} d\hat{q} e^{S_X} \int \prod_{a=1}^n d\Delta^a e^U, \quad (55)$$

where

$$S_X \doteq -N \left(\lambda\beta n \sum_{j \in \Psi_d} \bar{J}_j^2 + n\hat{Q}Q + \frac{n(n-1)}{2} \hat{q}q \right), \quad (56) \\ U \doteq -\lambda\beta \sum_a \|\Delta^a\|^2 +$$

$$\left(\hat{Q} - \frac{\hat{q}}{2}\right) \sum_a (\Delta^a)^T \Lambda \Delta^a + \frac{\hat{q}}{2} \sum_{a,b} (\Delta^a)^T \Lambda \Delta^b. \quad (57)$$

Note that in (57), different replicas Δ^a , Δ^b are coupled with each other, which makes it difficult to compute the integration. To overcome this problem, the Hubbard–Stratonovich transformation is used, i.e.,

$$e^{\frac{cy^2}{2}} = \frac{1}{\sqrt{2\pi c}} \int e^{-\frac{x^2}{2c} + xy} dx. \quad (58)$$

To apply it, we rewrite the term $\sum_{a,b} (\Delta^a)^T \Lambda \Delta^b$ as

$$\sum_{a,b} (\Delta^a)^T \Lambda \Delta^b = \sum_{a,b} \sum_i \gamma_i \Delta_i^a \Delta_i^b = \sum_i \gamma_i \left(\sum_a \Delta_i^a \right)^2 \quad (59)$$

so that

$$\begin{aligned} e^{\frac{\hat{q}}{2} \sum_{a,b} (\Delta^a)^T \Lambda \Delta^b} &= \prod_i e^{\frac{\gamma_i \hat{q} (\sum_a \Delta_i^a)^2}{2}} \\ &= \prod_i \int \frac{dz_i}{\sqrt{2\pi}} e^{-\frac{z_i^2}{2} + \sqrt{\gamma_i \hat{q}} z_i (\sum_a \Delta_i^a)} \\ &= \prod_i \int \mathcal{D}z_i e^{\sqrt{\gamma_i \hat{q}} z_i (\sum_a \Delta_i^a)}, \end{aligned} \quad (60)$$

where the change of variable $x_i = \sqrt{\gamma_i \hat{q}} z_i$ is applied and $\mathcal{D}z_i = \frac{dz_i}{\sqrt{2\pi}} e^{-\frac{z_i^2}{2}}$. Consequently, different replicas are decoupled and we have

$$\begin{aligned} \int \prod_{a=1}^n d\Delta^a e^U &= \int \prod_{a=1}^n d\Delta^a \exp\{-\lambda\beta \sum_a \|\Delta^a\|^2 \\ &\quad + \left(\hat{Q} - \frac{\hat{q}}{2}\right) \sum_a (\Delta^a)^T \Lambda \Delta^a\} \prod_i \int \mathcal{D}z_i e^{\sqrt{\gamma_i \hat{q}} z_i (\sum_a \Delta_i^a)} \\ &= \int \prod_i \mathcal{D}z_i \int \prod_{a=1}^n d\Delta^a \prod_a \exp\{-\lambda\beta \sum_i (\Delta_i^a)^2 \\ &\quad + \left(\hat{Q} - \frac{\hat{q}}{2}\right) \sum_i \gamma_i (\Delta_i^a)^2 + \sum_i \sqrt{\gamma_i \hat{q}} z_i \Delta_i^a\} \\ &= \int \prod_i \mathcal{D}z_i \int \prod_{a=1}^n d\Delta^a \prod_a \exp\left\{\sum_i \left[\left(\hat{Q} - \frac{\hat{q}}{2}\right) \gamma_i - \lambda\beta\right] (\Delta_i^a)^2\right. \end{aligned}$$

$$+ \sum_i \left(\sqrt{\gamma_i \hat{q} z_i} \right) \Delta_i^a \}. \quad (61)$$

Since

$$\int dx e^{-Ax^2+Bx} = \sqrt{\frac{\pi}{A}} e^{\frac{B^2}{4A}}, \quad (62)$$

then

$$\begin{aligned} & \int d\Delta_i^a \exp \left\{ \left[\left(\hat{Q} - \frac{\hat{q}}{2} \right) \gamma_i - \lambda\beta \right] (\Delta_i^a)^2 + \left(\sqrt{\gamma_i \hat{q} z_i} \right) \Delta_i^a \right\} \\ &= \sqrt{\frac{2\pi}{\gamma_i \left(\hat{q} - 2\hat{Q} + 2\lambda\beta/\gamma_i \right)}} \exp \left[\frac{1}{2} \frac{(\sqrt{\hat{q} z_i})^2}{\hat{q} - 2\hat{Q} + 2\lambda\beta/\gamma_i} \right]. \end{aligned} \quad (63)$$

Substituting (63) into (61), we have

$$\begin{aligned} \int \prod_{a=1}^n d\Delta^a e^U &= \int \prod_i \mathcal{D}z_i \times \\ & \exp \left\{ n \left[\sum_i \frac{1}{2} \frac{(\sqrt{\hat{q} z_i})^2}{\hat{q} - 2\hat{Q} + 2\lambda\beta/\gamma_i} + \frac{1}{2} \log 2\pi - \frac{1}{2} \log \gamma_i - \frac{1}{2} \log \left(\hat{q} - 2\hat{Q} + 2\lambda\beta/\gamma_i \right) \right] \right\}. \end{aligned} \quad (64)$$

Consequently, the original high-dimensional integration reduces to a product of one-dimensional integrations w.r.t. z_i , independently.

$$\int \mathcal{D}z_i \exp \left[\frac{1}{2} \frac{n (\sqrt{\hat{q} z_i})^2}{\hat{q} - 2\hat{Q} + 2\lambda\beta/\gamma_i} \right] = \sqrt{\frac{1}{1 - \frac{n\hat{q}}{\hat{q} - 2\hat{Q} + 2\lambda\beta/\gamma_i}}}. \quad (65)$$

Then, we obtain

$$\begin{aligned} \int \prod_{a=1}^n d\Delta^a e^U &= \exp \left\{ -\frac{1}{2} \sum_i \log \left(1 - \frac{n\hat{q}}{\hat{q} - 2\hat{Q} + 2\lambda\beta/\gamma_i} \right) \right. \\ & \left. + \frac{N}{2} \log 2\pi - \frac{1}{2} \sum_i \log \gamma_i - \frac{1}{2} \sum_i \log \left(\hat{q} - 2\hat{Q} + 2\lambda\beta/\gamma_i \right) \right\}. \end{aligned} \quad (66)$$

Thus,

$$\lim_{n \rightarrow 0} \frac{S}{n} = \text{Extr}_{\hat{q}, \hat{Q}} \left\{ \lim_{n \rightarrow 0} \frac{\log \int d\hat{Q} d\hat{q} e^{Sx} \int \prod_{a=1}^n d\Delta^a e^U}{Nn} \right\}$$

$$\begin{aligned}
 &= \text{Extr}_{\hat{q}, \hat{Q}} \left\{ - \left(\lambda \beta \sum_{j \in \Psi_d} \bar{J}_j^2 + \hat{Q}Q - \frac{1}{2} \hat{q}q \right) + \frac{\hat{q}}{2N} \sum_i \frac{1}{\hat{q} - 2\hat{Q} + 2\lambda\beta/\gamma_i} \right. \\
 &\quad \left. + \frac{1}{2} \log 2\pi - \frac{1}{2N} \sum_i \log \gamma_i - \frac{1}{2N} \sum_i \log \left(\hat{q} - 2\hat{Q} + 2\lambda\beta/\gamma_i \right) \right\}, \quad (67)
 \end{aligned}$$

where $\text{Extr}_{\hat{q}, \hat{Q}}\{\cdot\}$ denotes the extreme operation over \hat{q}, \hat{Q} . The summation in (67) is difficult to calculate. However, in the large system limit, the summation converges to the integration, which leads to

$$\begin{aligned}
 \lim_{n \rightarrow 0} \frac{S}{n} &= \text{Extr}_{\hat{q}, \hat{Q}} \left\{ - \left(\lambda \beta \sum_{j \in \Psi_d} \bar{J}_j^2 + \hat{Q}Q - \frac{1}{2} \hat{q}q \right) + \frac{\hat{q}}{2\beta} G_1 \left(\frac{\hat{q} - 2\hat{Q}}{\beta} \right) \right. \\
 &\quad \left. + \frac{1}{2} \log 2\pi - \frac{1}{2N} \text{Tr} \log \left(\mathbf{C}^{\setminus 0} \right)^{-1} - \frac{1}{2} G_2 \left(\frac{\hat{q} - 2\hat{Q}}{\beta} \right) - \frac{1}{2} \log \beta \right\}, \quad (68)
 \end{aligned}$$

where

$$G_1(x) = \int \frac{d\eta \rho(\eta)}{x + 2\lambda\eta}, \quad (69)$$

$$G_2(x) = \int d\eta \rho(\eta) \log(x + 2\lambda\eta). \quad (70)$$

Consequently, extremization w.r.t. $\hat{q}, \hat{Q}, \hat{m}$ leads to

$$\begin{cases} q = -\frac{\hat{q}}{\beta^2} G_1' \left(\frac{\hat{q} - 2\hat{Q}}{\beta} \right), \\ Q - q = \frac{1}{\beta} G_1 \left(\frac{\hat{q} - 2\hat{Q}}{\beta} \right). \end{cases} \quad (71)$$

Therefore, we obtain

$$\begin{aligned}
 \lim_{n \rightarrow 0} \frac{S}{n} &= -\lambda\beta \sum_{j \in \Psi_d} \bar{J}_j^2 + \frac{Q\beta}{2} G_1^{-1}(\beta(Q - q)) - \frac{1}{2} G_2(G_1^{-1}(\beta(Q - q))) \\
 &\quad + \frac{1}{2} \log \frac{2\pi}{\beta} - \frac{1}{2N} \text{Tr} \log \left(\mathbf{C}^{\setminus 0} \right)^{-1}. \quad (72)
 \end{aligned}$$

Appendix B Computation of L

The definition of L is given in (31), which is

$$L \doteq \sum_{s_0, \mathbf{s}_{\Psi_d}} P(s_0, \mathbf{s}_{\Psi_d} | J^*) \int \prod_{a=1}^n dh_{\Delta}^a P_{\text{cav}} \left(\{h_{\Delta}^a\}_a \mid \{\Delta^a\}_a \right) e^{-\beta \sum_{a=1}^n \Phi \left(s_0 \left(\sum_{j \in \Psi_d} \bar{J}_j s_j + h_{\Delta}^a \right) \right)}. \quad (73)$$

Using the cavity method, the local fields $h_{\Delta}^a, a = 1, \dots, n$ follow a joint Gaussian distribution with zero mean (paramagnetic assumption) and covariances as

$$\langle h_a h_b \rangle \setminus^0 = Q \delta_{ab} + (1 - \delta_{ab}) q. \quad (74)$$

Then, we can introduce two auxiliary i.i.d. Gaussian random variables v_a, z with zero mean and unit variance, by which the local fields can be written in a compact form

$$h_a = \sqrt{Q - q} v_a + \sqrt{q} z \quad (75)$$

so that L in (73) can be equivalently written as

$$\begin{aligned} L &\doteq \sum_{s_0, \mathbf{s}_{\Psi_d}} P(s_0, \mathbf{s}_{\Psi_d} | J^*) \int \prod_{a=1}^n dh_{\Delta}^a P_{\text{cav}} \left(\{h_{\Delta}^a\}_a \mid \{\Delta^a\}_a \right) e^{-\beta \sum_{a=1}^n \Phi \left(s_0 \left(\sum_{j \in \Psi_d} \bar{J}_j s_j + h_{\Delta}^a \right) \right)} \\ &= \sum_{s_0, \mathbf{s}_{\Psi_d}} P(s_0, \mathbf{s}_{\Psi_d} | J^*) \int \mathcal{D}z \prod_a \mathcal{D}v_a e^{-\beta \sum_{a=1}^n \Phi \left(s_0 \left(\sum_{j \in \Psi_d} \bar{J}_j s_j + \sqrt{Q - q} v_a + \sqrt{q} z \right) \right)} \\ &= \sum_{s_0, \mathbf{s}_{\Psi_d}} P(s_0, \mathbf{s}_{\Psi_d} | J^*) \int \mathcal{D}z \left[\underbrace{\int \mathcal{D}v e^{-\beta \Phi \left(s_0 \left(\sum_{j \in \Psi_d} \bar{J}_j s_j + \sqrt{Q - q} v + \sqrt{q} z \right) \right)}}_A \right]^n \\ &= \sum_{s_0, \mathbf{s}_{\Psi_d}} P(s_0, \mathbf{s}_{\Psi_d} | J^*) E_z(A^n), \end{aligned} \quad (76)$$

where $E_z(A^n) = \int \mathcal{D}z A^n$. Then, using the replica formula, we have

$$\begin{aligned} \lim_{n \rightarrow 0} \frac{1}{n} \log L &= \lim_{n \rightarrow 0} \frac{\log \sum_{s_0, \mathbf{s}_{\Psi_d}} P(s_0, \mathbf{s}_{\Psi_d} | J^*) E_z(A^n)}{n} \\ &= E_z \left[\sum_{s_0, \mathbf{s}_{\Psi_d}} P(s_0, \mathbf{s}_{\Psi_d} | J^*) A \right] \\ &= \sum_{s_0, \mathbf{s}_{\Psi_d}} P(s_0, \mathbf{s}_{\Psi_d} | J^*) \int \mathcal{D}z \log \int \mathcal{D}v e^{-\beta \Phi \left(s_0 \left(\sum_{j \in \Psi_d} \bar{J}_j s_j + \sqrt{Q - q} v + \sqrt{q} z \right) \right)}. \end{aligned} \quad (77)$$

To further simplify the result, let $y = s_0 \left(\sum_{j \in \Psi_d} \bar{J}_j s_j + \sqrt{Q - q}v + \sqrt{q}z \right)$. Consequently, we obtain

$$\begin{aligned}
 & \int \mathcal{D}v e^{-\beta \Phi(s_0(\sum_{j \in \Omega} \bar{J}_j s_j + \sqrt{Q - q}v + \sqrt{q}z))} \\
 &= \int \frac{dv}{\sqrt{2\pi}} e^{-\frac{v^2}{2}} e^{-\beta \Phi(y)} \\
 &= \int \frac{dy}{\sqrt{2\pi(Q - q)}} e^{-\frac{[y - s_0(\sum_{j \in \Omega} \bar{J}_j s_j + \sqrt{q}z)]^2}{2(Q - q)}} e^{-\beta \Phi(y)}, \tag{78}
 \end{aligned}$$

so that

$$\begin{aligned}
 \lim_{n \rightarrow 0} \frac{1}{n} \log L &= \sum_{s_0, \mathbf{s}_{\Psi_d}} P(s_0, \mathbf{s}_{\Psi_d} | J^*) \int \mathcal{D}z \log \int \frac{dy}{\sqrt{2\pi(Q - q)}} e^{-\frac{[y - s_0(\sum_{j \in \Psi_d} \bar{J}_j s_j + \sqrt{q}z)]^2}{2(Q - q)}} e^{-\beta \Phi(y)} \\
 &= \sum_{s_0, \mathbf{s}_{\Psi_d}} P(s_0, \mathbf{s}_{\Psi_d} | J^*) \int \mathcal{D}z \max_y \left[-\frac{\left(y - s_0 \left(\sqrt{q}z + \sum_{j \in \Psi_d} \bar{J}_j s_j \right) \right)^2}{2(Q - q)} - \beta \Phi(y) \right]. \tag{79}
 \end{aligned}$$

Appendix C Derivation of Macroscopic Parameters

We use the technique of auxiliary variables in Bachschmid-Romano and Opper (2017) by introducing the term $h_R \sum_{a=1}^n \|\mathbf{W}^a\|^2$ into $[Z^n]_{\mathcal{D}M}$. Then, following the same procedure as that in Appendix Appendix A, we obtain

$$\begin{aligned}
 \lim_{n \rightarrow 0} \frac{S}{n} &= \text{Extr}_{\hat{q}, \hat{Q}} \left\{ -\lambda \beta \sum_{j \in \Psi_d} \bar{J}_j^2 - \hat{Q}Q + \frac{1}{2} \hat{q}q + \frac{1}{2} \frac{1}{N} \sum_i \frac{\gamma_i \hat{q}}{(\hat{q} - 2\hat{Q}) \gamma_i + 2(\lambda \beta - h_R)} \right. \\
 &\quad \left. - \frac{1}{2N} \sum_i \log \left(\hat{q} - 2\hat{Q} + 2(\lambda \beta - h_R) / \gamma_i \right) - \frac{1}{2N} \sum_i \log \gamma_i \right\}. \tag{80}
 \end{aligned}$$

Thus, the macroscopic parameter $R = \frac{1}{N} \sum_{j \in \bar{\Psi}_d} \Delta_j^2$ can be derived using the derivative of the free energy, i.e.,

$$\begin{aligned}
 R &= \lim_{h_R \rightarrow 0} \frac{\partial}{\partial h_R} \lim_{n \rightarrow 0} \frac{S}{n} \\
 &= \frac{1}{N} \sum_i \frac{\hat{q} / \gamma_i}{\left(\hat{q} - 2\hat{Q} + 2\lambda \beta / \gamma_i \right)^2} + \frac{1}{N} \sum_i \frac{1 / \gamma_i}{\hat{q} - 2\hat{Q} + 2\lambda \beta / \gamma_i}
 \end{aligned}$$

$$\begin{aligned}
 &= \frac{\hat{q}}{\beta^2} \frac{1}{N} \sum_i \frac{1/\gamma_i}{\left(\frac{\hat{q}-2\hat{Q}}{\beta} + 2\lambda/\gamma_i\right)^2} + \frac{1}{\beta} \frac{1}{N} \sum \frac{1/\gamma_i}{\frac{\hat{q}-2\hat{Q}}{\beta} + 2\lambda/\gamma_i} \\
 &= \frac{\hat{q}}{\beta^2} \frac{1}{N} \sum_i \frac{1/\gamma_i}{\left(\frac{\hat{q}-2\hat{Q}}{\beta} + 2\lambda/\gamma_i\right)^2} + \underbrace{\frac{1}{\beta} \frac{1}{N} \sum \frac{1/\gamma_i}{a + 2\lambda/\gamma_i}}_{\rightarrow 0 \ (\beta \rightarrow \infty)} \\
 &= q \frac{G'_3(\kappa)}{G'_1(\kappa)},
 \end{aligned} \tag{81}$$

where

$$G_3(x) = \int \frac{d\eta \rho(\eta) \eta}{(x + 2\lambda\eta)}. \tag{82}$$

Appendix D Numerical Solutions

In general, there is no analytic solution to the EOS equations in Section 3.3, but they can be easily solved using numerical methods.

First, we compute \hat{y} by substituting $\Phi(y) = (y-1)^2$ into (40), which yields

$$\hat{y} = \frac{s_0 \left(\sqrt{Q}z + \sum_{j \in \Psi_d} \bar{J}_j s_j \right) + 2G_1(\kappa)}{1 + 2G_1(\kappa)}, \tag{83}$$

from which we obtain

$$\begin{cases} \int \mathcal{D}z \frac{\partial \Phi(y)}{\partial y} \Big|_{y=\hat{y}} = 2 \frac{s_0 \sum_{j \in \Psi_d} \bar{J}_j s_j - 1}{1 + 2G_1(\kappa)}, \\ \int \mathcal{D}z z \frac{\partial \Phi(y)}{\partial y} \Big|_{y=\hat{y}} = \frac{2s_0 \sqrt{Q}}{1 + 2G_1(\kappa)}, \\ \int \mathcal{D}z \left(\frac{\partial \Phi(y)}{\partial y} \Big|_{y=\hat{y}} \right)^2 = 4 \frac{Q + \left(\sum_{j \in \Psi_d} \bar{J}_j s_j \right)^2 - 2s_0 \left(\sum_{j \in \Psi_d} \bar{J}_j s_j \right) + 1}{[1 + 2G_1(\kappa)]^2}. \end{cases} \tag{84}$$

The mean estimates $(\bar{J}_j)_{j \in \Psi_d}$ can also be evaluated by the extremization condition, i.e.,

$$0 = 2\lambda \bar{J}_j + \alpha \sum_{s_0, \mathbf{s}_{\Psi_d}} P(s_0, \mathbf{s}_{\Psi_d} | J^*) \int \mathcal{D}z \frac{\partial \Phi(y)}{\partial y} \Big|_{y=\hat{y}} s_0 s_j, \quad j \in \Psi_d. \tag{85}$$

Hence, the mean estimates $(\bar{J}_j)_{j \in \Psi_d}$ can be evaluated from (85) by solving the linear equations

$$(1 + 2\lambda/\kappa) \bar{J}_j + \sum_{i \in \Psi_d, i \neq j} \bar{J}_i \langle s_i s_j \rangle - \langle s_0 s_j \rangle = 0, \quad j \in \Psi_d, \tag{86}$$

where $\langle s_i s_j \rangle$ denotes the average w.r.t. the joint distribution $P(s_0, \mathbf{s}_{\Psi_d} | J^*)$.

The macroscopic parameters κ and Q can be obtained by numerically solving the following equations

$$0 = \kappa - \frac{2\alpha}{1 + 2G_1(\kappa)}, \quad (87)$$

$$Q = \frac{4\alpha G_1'(\kappa) \left(2 \left\langle s_0 \sum_{j \in \Psi_d} \bar{J}_j s_j \right\rangle - \left\langle \left(\sum_{j \in \Psi_d} \bar{J}_j s_j \right)^2 \right\rangle - 1 \right)}{(1 + 2G_1(\kappa))^2 + 4\alpha G_1'(\kappa)}. \quad (88)$$

Appendix E Eigenvalue Distribution

From the replica analysis presented, the learning performance will depend on the eigenvalue distribution (EVD) $\rho(\eta)$ of the inverse correlation matrix $(\mathbf{C}^{\setminus 0})^{-1}$. In general, it is difficult to obtain this EVD; however, for a particular teacher network, we can obtain the analytic solution of $\rho(\eta)$. In this section, we illustrate how to compute $\rho(\eta)$ of the random regular (RR) graph as a representative example of sparse tree-like graphs. Assume that as $N \rightarrow \infty$, the EVD of $(\mathbf{C}^{\setminus 0})^{-1}$ approaches that of \mathbf{C}^{-1} in the large system limit, where \mathbf{C} is the correlation matrix that corresponds to the teacher spin system. The Gibbs free energy is defined as

$$G(\mathbf{m}) = \max_{\boldsymbol{\theta}} \{ \boldsymbol{\theta}^T \mathbf{m} - \log Z(\boldsymbol{\theta}) \}, \quad (89)$$

where $Z(\boldsymbol{\theta}) = \sum_{\mathbf{s}} e^{\sum_{i < j} J_{ij} s_i s_j + \sum_i \theta_i s_i}$. It can be verified that the Hessian of $G(\mathbf{m})$ is equal to the inverse correlation matrix, i.e., $[\mathbf{C}^{-1}]_{ij} = \frac{\partial^2 G(\mathbf{m})}{\partial m_i \partial m_j}$. Consequently, we can focus on the computation of $G(\mathbf{m})$ to obtain the EVD of \mathbf{C}^{-1} . The RR graph is characterized by a connectivity parameter c and constant coupling strength K . The inverse correlation matrix can be computed from the Hessian of the Gibbs free energy (Ricci-Tersenghi, 2012; Nguyen and Berg, 2012; Abbara et al., 2020) as

$$\begin{aligned} [\mathbf{C}^{-1}]_{ij} &= \frac{\partial^2 G(\mathbf{m})}{\partial m_i \partial m_j} \\ &= \left(\frac{c}{1 - \tanh^2 K} - c + 1 \right) \delta_{ij} - \frac{\tanh(J_{ij})}{1 - \tanh^2(J_{ij})} (1 - \delta_{ij}), \end{aligned} \quad (90)$$

and in matrix form, we have

$$\mathbf{C}^{-1} = \left(\frac{c}{1 - \tanh^2 K} - c + 1 \right) \mathbf{I} - \frac{\tanh(\mathbf{J})}{1 - \tanh^2(\mathbf{J})}. \quad (91)$$

Since the matrix $\frac{\tanh(\mathbf{J})}{1 - \tanh^2(\mathbf{J})}$ is also a sparse coupling matrix with constant coupling strength $K_1 = \frac{\tanh(K)}{1 - \tanh^2(K)}$ and fixed connectivity c , the corresponding eigenvalue (denoted as ξ)

distribution can be calculated as (McKay, 1981)

$$\rho_\xi(\xi) = \frac{c\sqrt{4K_1^2(c-1) - \xi^2}}{2\pi(K_1^2c^2 - \xi^2)}, \quad |\xi| \leq 2K_1\sqrt{c-1}. \quad (92)$$

From (91), the eigenvalue η of \mathbf{C}^{-1} is

$$\eta_i = \frac{c}{1 - \tanh^2 K} - c + 1 - \xi_i, \quad (93)$$

which, when combined with (92), readily yields the EVD of η as $N \rightarrow \infty$ as follows:

$$\begin{aligned} \rho(\eta) &= \rho_\xi \left(\frac{c}{1 - \tanh^2 K} - c + 1 - \eta \right) \\ &= \frac{c\sqrt{4\left(\frac{\tanh(K)}{1 - \tanh^2(K)}\right)^2(c-1) - \left(\frac{c}{1 - \tanh^2 K} - c + 1 - \eta\right)^2}}{2\pi\left(\left(\frac{\tanh(K)}{1 - \tanh^2(K)}\right)^2c^2 - \left(\frac{c}{1 - \tanh^2 K} - c + 1 - \eta\right)^2\right)}, \end{aligned} \quad (94)$$

where $\eta \in \left[\frac{c}{1 - \tanh^2 K} - c + 1 - \frac{2\tanh(K)\sqrt{c-1}}{1 - \tanh^2(K)}, \frac{c}{1 - \tanh^2 K} - c + 1 + \frac{2\tanh(K)\sqrt{c-1}}{1 - \tanh^2(K)} \right]$.

Appendix F Proof of Theorem 1

Proof Although the proof in the previous study (the one in Sec. 3.3 in Abbara et al. (2020)) can be applied to the present case, we provide another proof by employing some specific properties of the linear regression, because some steps in this proof are essential for Theorem 2, which is beyond the applicable range of the proof in Abbara et al. (2020). Note that the advantage of the proof in Abbara et al. (2020) is its generality: an arbitrary cost function and the nonzero external fields are treated.

Specifically, in this case, the linear equations in (46) reduce to

$$\sum_{i \in \Psi_d} \bar{J}_i \langle s_i s_j \rangle = \langle s_0 s_j \rangle, \quad j \in \Psi_d. \quad (95)$$

In matrix form,

$$\begin{aligned} \mathbf{C}_d \bar{\mathbf{J}} &= \mathbf{b}, \quad (96) \\ \bar{\mathbf{J}} &= \begin{bmatrix} \bar{J}_1 \\ \bar{J}_2 \\ \vdots \\ \bar{J}_{|\Psi_d|} \end{bmatrix}, \quad \mathbf{b} = \begin{bmatrix} \langle s_0 s_1 \rangle \\ \langle s_0 s_2 \rangle \\ \vdots \\ \langle s_0 s_{|\Psi_d|} \rangle \end{bmatrix}, \quad (97) \end{aligned}$$

where $\mathbf{C}_d = \{\langle s_i s_j \rangle\}_{i,j \in \Psi_d}$ is the correlation matrix of spins $s_j, j \in \Psi_d$. Consequently, the estimates $\bar{\mathbf{J}} = (\bar{J}_j)_{j \in \Psi_d}$ can be computed as $\bar{\mathbf{J}} = \mathbf{C}_d^{-1} \mathbf{b}$.

On the one hand, the full correlation matrix $\mathbf{C}_{0d} = \{\langle s_i s_j \rangle\}_{i,j \in \{0, \Psi_d\}}$ of spins $s_j, j \in \{0, \Psi_d\}$ can be represented as

$$\mathbf{C}_{0d} = \begin{bmatrix} 1 & \mathbf{b}^T \\ \mathbf{b} & \mathbf{C}_d \end{bmatrix}. \quad (98)$$

Thus, according to the block matrix inversion lemma, the inverse correlation matrix can be computed as

$$\mathbf{C}_{0d}^{-1} = \begin{bmatrix} F_{11}^{-1} & -F_{11}^{-1} \bar{\mathbf{J}}^T \\ -\bar{\mathbf{J}} F_{11}^{-1} & F_{22}^{-1} \end{bmatrix}, \quad (99)$$

where $F_{11} = 1 - \mathbf{b}^T \bar{\mathbf{J}}, F_{22} = \mathbf{C}_d - \mathbf{b} \mathbf{b}^T$.

On the other hand, for a sparse tree graph where s_i has connectivity c_i with true coupling J_{ij} with spin s_j , the inverse correlation matrix can be computed from the Hessian of the Gibbs free energy as (Ricci-Tersenghi, 2012; Nguyen and Berg, 2012; Abbara et al., 2020)

$$[\mathbf{C}_{0d}^{-1}]_{ij} = \left(\sum_{k \in \partial i} \frac{1}{1 - \tanh^2 J_{ik}} - c_i + 1 \right) \delta_{ij} - \frac{\tanh(J_{ij})}{1 - \tanh^2 J_{ij}} (1 - \delta_{ij}). \quad (100)$$

The two representations of \mathbf{C}_{0d}^{-1} in (99) and (100) are equivalent; hence, the corresponding elements should be equal to each other. Specifically, we are interested in the first row, which corresponds to spin s_0 . Denote $J_{0j} = J_j^*$ as the true couplings associated with spin s_0 in the teacher network. Then, by the definition of Ω_1 , we have $J_j^* = 0, j \notin \Omega_1$. Assuming that $c_0 = c = |\Omega_1|$, by comparing (99) and (100), it is easy to obtain

$$F_{11}^{-1} = \sum_{k \in \Omega_1} \frac{1}{1 - \tanh^2 J_k^*} - c + 1, \quad (101)$$

$$\bar{J}_j F_{11}^{-1} = \frac{\tanh(J_j^*)}{1 - \tanh^2(J_j^*)}, \quad (102)$$

which is the same as (47). The result of (48) can be readily obtained for constant couplings by substituting $J_j^* = K \text{sign}(J_j^*), j \in \Omega_1$, which completes the proof. \blacksquare

Appendix G Proof of Theorem 2

Proof In this case, the estimate of $\bar{\mathbf{J}} = (\bar{J}_j)_{j \in \Psi_d}$ is the solution to the following linear equations:

$$\left(\mathbf{C}_d + \frac{2\lambda}{\kappa} \mathbf{I} \right) \bar{\mathbf{J}} = \mathbf{b}, \quad (103)$$

where \mathbf{I} is the identity matrix. To evaluate the decay speed of $(\bar{J}_j)_{j \in \Psi_d}$ with the distance from s_0 , we can compute the decay speed of $(\bar{J}_j)_{j \in \Psi_d}$ for two general NN spins s_i and s_j with distance 1. For notational simplicity, denote $\text{Dist}(s_i, s_j)$ as the distance between two spins s_i and s_j in the teacher Ising system. Then, for two NN spins s_i and s_j , $\text{Dist}(s_i, s_j) = 1$. Without loss of generality, using the gauge symmetry, we can assume that all the true couplings of the teacher Ising spin system are non-negative when the external field is absent and the paramagnet assumption holds; hence, each element in \mathbf{C}_d and \mathbf{b} is positive. Assuming that $\text{Dist}(s_i, s_0) = d-1$ and $\text{Dist}(s_j, s_0) = d$, then $\langle s_0 s_i \rangle = \theta^{d-1}$ and $\langle s_0 s_j \rangle = \theta^d$. In general, there are two cases.

Case 1: s_j is a leaf spin, which means that s_j is only directly connected to its parent spin s_i and has no children spins.

In this case, for any other spin $s_k, k \in \Psi_d, k \neq j$, we have $\text{Dist}(s_j, s_k) = \text{Dist}(s_i, s_k) + 1$. Then, the associated rows corresponding to s_i and s_j in (103) can be written as follows:

$$\begin{cases} \left(1 + \frac{2\lambda}{\kappa}\right) \bar{J}_i + \theta \bar{J}_j + \sum_{k \in \Psi_d, k \neq i, j} \theta^{d_{ki}} \bar{J}_k = \theta^{d-1}, \\ \theta \bar{J}_i + \left(1 + \frac{2\lambda}{\kappa}\right) \bar{J}_j + \sum_{k \in \Psi_d, k \neq i, j} \theta^{d_{ki}+1} \bar{J}_k = \theta^d, \end{cases}, \quad (104)$$

where $d_{ki} = \text{Dist}(s_i, s_k)$ and $d_{kj} = \text{Dist}(s_j, s_k)$. From (104), we can easily obtain

$$0 < \frac{\bar{J}_j}{\bar{J}_i} = \theta \frac{(D-1)}{D-\theta^2} < \theta, \quad (105)$$

where $D = 1 + \frac{2\lambda}{\kappa} > 1$, which implies that the ratio of the magnitude of \bar{J}_j to that of its parent node \bar{J}_i is smaller than θ whenever s_j is a leaf spin. Meanwhile, the signs of \bar{J}_j and \bar{J}_i are always the same, i.e., s_i has the same sign as its children spin s_j when s_j is a leaf spin.

Case 2: s_j is not a leaf spin but has its own direct children spins.

Denote Φ as the set of children spins of s_j . Then, for any spin $s_m, m \in \Phi$, we have $\text{Dist}(s_j, s_m) = \text{Dist}(s_i, s_m) - 1$. For any other spin $s_k, k \in \Psi_d/\Phi, k \neq j$, we have $\text{Dist}(s_j, s_k) = \text{Dist}(s_i, s_k) + 1$. Consequently, the associated rows corresponding to s_i and s_j in (103) can be written as follows:

$$\begin{cases} \left(1 + \frac{2\lambda}{\kappa}\right) \bar{J}_i + \theta \bar{J}_j + \sum_{k \in \Psi_d/\Phi, k \neq i, j} \theta^{d_{ki}} \bar{J}_k + \sum_{m \in \Phi} \theta^{d_{mj}+1} \bar{J}_m = \theta^{d-1}, \\ \theta \bar{J}_i + \left(1 + \frac{2\lambda}{\kappa}\right) \bar{J}_j + \sum_{k \in \Psi_d/\Phi, k \neq i, j} \theta^{d_{ki}+1} \bar{J}_k + \sum_{m \in \Phi} \theta^{d_{mj}} \bar{J}_m = \theta^d. \end{cases} \quad (106)$$

Then, denoting $D = 1 + \frac{2\lambda}{\kappa} > 1$, we obtain

$$\frac{\bar{J}_i}{\bar{J}_j} = \frac{D - \theta^2}{\theta(D - 1)} + \frac{1}{\bar{J}_j} \sum_{m \in \Phi} \bar{J}_m \left(\theta^{d_{mj}} - \theta^{d_{mj}+2} \right). \quad (107)$$

Since Φ is the set of children spins of s_j , then for any $\bar{J}_m, m \in \Phi$, it can be deduced by induction that \bar{J}_m has the same sign as \bar{J}_j as follows.

First, if $s_m, m \in \Phi$ are all leaf spins, then using the result of case 1, \bar{J}_m has the same sign as \bar{J}_j , i.e., $\bar{J}_m/\bar{J}_j > 0$. Second, if $s_m, m \in \Phi$ is not a leaf spin itself but has a leaf spin s_n , then \bar{J}_n has the same sign as \bar{J}_m , and as with (107), we can obtain $\bar{J}_j/\bar{J}_m = \frac{D-\theta^2}{\theta(D-1)} + \frac{1}{\bar{J}_m} \bar{J}_n (\theta - \theta^2) > 0$; hence, \bar{J}_m has the same sign as \bar{J}_j . By induction, the estimates of the children spins $\bar{J}_m, m \in \Phi$ will all have the same sign as \bar{J}_j .

Consequently, since (107), $\bar{J}_m/\bar{J}_j > 0, m \in \Phi$, and $0 < \theta < 1$, we have

$$\frac{\bar{J}_i}{\bar{J}_j} > \frac{D - \theta^2}{\theta(D - 1)} > 0 \iff 0 < \frac{\bar{J}_j}{\bar{J}_i} < \frac{\theta(D - 1)}{D - \theta^2}, \quad (108)$$

which implies that the ratio of the magnitude of \bar{J}_j to that of its parent spin \bar{J}_i is smaller than $\frac{\theta(D-1)}{D-\theta^2}$ for general s_j when it is not a leaf spin.

Summarizing both case 1 and case 2, for any two spins s_i and s_j with distance $\text{Dist}(s_i, s_j) = 1$, $\left| \frac{\bar{J}_j}{\bar{J}_i} \right| \leq \frac{\theta(D-1)}{D-\theta^2}$ always holds, which completes the proof. \blacksquare

References

- A. Abbara, Y. Kabashima, T. Obuchi, and Y. Xu. Learning performance in inverse ising problems with sparse teacher couplings. *Journal of Statistical Mechanics: Theory and Experiment*, 2020(7):073402, 2020.
- D. H. Ackley, G. E. Hinton, and T. J. Sejnowski. A learning algorithm for boltzmann machines. *Cognitive science*, 9(1):147–169, 1985.
- E. Aurell and M. Ekeberg. Inverse ising inference using all the data. *Physical review letters*, 108(9):090201, 2012.
- L. Bachschmid-Romano and M. Opper. Learning of couplings for random asymmetric kinetic ising models revisited: random correlation matrices and learning curves. *Journal of Statistical Mechanics: Theory and Experiment*, 2015(9):P09016, 2015.
- L. Bachschmid-Romano and M. Opper. A statistical physics approach to learning curves for the inverse ising problem. *Journal of Statistical Mechanics: Theory and Experiment*, 2017(6):063406, 2017.

- J. Berg. Statistical mechanics of the inverse ising problem and the optimal objective function. *Journal of Statistical Mechanics: Theory and Experiment*, 2017(8):083402, 2017.
- J. Besag. Statistical analysis of non-lattice data. *Journal of the Royal Statistical Society: Series D (The Statistician)*, 24(3):179–195, 1975.
- G. Bresler. Efficiently learning ising models on arbitrary graphs. In *Proceedings of the forty-seventh annual ACM symposium on Theory of computing*, pages 771–782, 2015.
- T. Broderick, M. Dudik, G. Tkacik, R. E. Schapire, and W. Bialek. Faster solutions of the inverse pairwise ising problem. *arXiv preprint arXiv:0712.2437*, 2007.
- A. Decelle and F. Ricci-Tersenghi. Pseudolikelihood decimation algorithm improving the inference of the interaction network in a general class of ising models. *Physical review letters*, 112(7):070603, 2014.
- M. Habeck. Bayesian approach to inverse statistical mechanics. *Physical Review E*, 89(5):052113, 2014.
- A. Hyvärinen. Consistency of pseudolikelihood estimation of fully visible boltzmann machines. *Neural Computation*, 18(10):2283–2292, 2006.
- H. J. Kappen and F. d. B. Rodríguez. Efficient learning in boltzmann machines using linear response theory. *Neural Computation*, 10(5):1137–1156, 1998.
- A. Y. Lokhov, M. Vuffray, S. Misra, and M. Chertkov. Optimal structure and parameter learning of ising models. *Science advances*, 4(3):e1700791, 2018.
- B. D. McKay. The expected eigenvalue distribution of a large regular graph. *Linear Algebra and its Applications*, 40:203–216, 1981.
- M. Mezard and A. Montanari. *Information, physics, and computation*. Oxford University Press, 2009.
- A. Mozeika, O. Dikmen, and J. Piili. Consistent inference of a general model using the pseudolikelihood method. *Physical Review E*, 90(1):010101, 2014.
- H. C. Nguyen and J. Berg. Bethe–peierls approximation and the inverse ising problem. *Journal of Statistical Mechanics: Theory and Experiment*, 2012(03):P03004, 2012.
- H. C. Nguyen, R. Zecchina, and J. Berg. Inverse statistical problems: from the inverse ising problem to data science. *Advances in Physics*, 66(3):197–261, 2017.
- H. Nishimori. *Statistical physics of spin glasses and information processing: an introduction*. Number 111. Clarendon Press, 2001.

- M. Opper and D. Saad. *Advanced mean field methods: Theory and practice*. MIT press, 2001.
- P. Ravikumar, M. J. Wainwright, J. D. Lafferty, et al. High-dimensional ising model selection using ℓ_1 -regularized logistic regression. *The Annals of Statistics*, 38(3):1287–1319, 2010.
- F. Ricci-Tersenghi. The bethe approximation for solving the inverse ising problem: a comparison with other inference methods. *Journal of Statistical Mechanics: Theory and Experiment*, 2012(08):P08015, 2012.
- N. P. Santhanam and M. J. Wainwright. Information-theoretic limits of selecting binary graphical models in high dimensions. *IEEE Transactions on Information Theory*, 58(7):4117–4134, 2012.
- M. Schmidt, A. Niculescu-Mizil, K. Murphy, et al. Learning graphical model structure using ℓ_1 -regularization paths. In *AAAI*, volume 7, pages 1278–1283, 2007.
- V. Sessak and R. Monasson. Small-correlation expansions for the inverse ising problem. *Journal of Physics A: Mathematical and Theoretical*, 42(5):055001, 2009.
- T. Tanaka. Mean-field theory of boltzmann machine learning. *Physical Review E*, 58(2):2302, 1998.
- R. Tibshirani. Regression shrinkage and selection via the lasso. *Journal of the Royal Statistical Society: Series B (Methodological)*, 58(1):267–288, 1996.
- M. Vuffray, S. Misra, A. Lokhov, and M. Chertkov. Interaction screening: Efficient and sample-optimal learning of ising models. In *Advances in Neural Information Processing Systems*, pages 2595–2603, 2016.
- M. J. Wainwright and M. I. Jordan. *Graphical models, exponential families, and variational inference*. Now Publishers Inc, 2008.